Astronomy & Astrophysics manuscript no. 4921
February 5, 2008

XMM–Newton observations of a sample of γ–ray loud active galactic nuclei⋆

L. Foschini[1], G. Ghisellini[2], C.M. Raiteri[3], F. Tavecchio[2], M. Villata[3], L. Maraschi[2], E. Pian[4], G. Tagliaferri[2], G. Di Cocco[1], G. Malaguti[1]

[1] INAF/IASF-Bologna, Via Gobetti 101, 40129, Bologna (Italy)
[2] INAF, Osservatorio Astronomico di Brera, Via Bianchi 46, 23807, Merate (Italy)
[3] INAF, Osservatorio Astronomico di Torino, Via Osservatorio 20, 10025, Pino Torinese (Italy)
[4] INAF, Osservatorio Astronomico di Trieste, Via G.B. Tiepolo 11, 34131, Trieste (Italy)

Received 27 January 2006; Accepted 9 March 2006

ABSTRACT

Aims. To understand the nature of γ–ray loud active galactic nuclei (AGN) and the mechanisms for the generation of high-energy γ–rays.
Methods. We performed a homogeneous and systematic analysis of simultaneous X-ray and optical/UV properties of a group of 15 γ–ray loud AGN, using observations performed with *XMM-Newton*. The sample is composed of 13 blazars (6 BL Lac and 7 Flat-Spectrum Radio Quasar) and 2 radio galaxies that are associated with detections at energies > 100 MeV. The data for 7 of them are analyzed here for the first time, including the first X-ray observation of PKS 1406 – 706. The spectral characteristics of the sources in the present sample were compared with those in previous catalogs of blazars and other AGN, to search for difference or long term changes.
Results. All the selected sources appear to follow the classic "blazar sequence" and the spectral energy distributions (SED) built with the present X-ray and optical/UV data and completed with historical data, confirm the findings of previous studies on this type of source. Some sources display interesting features: four of them, namely AO 0235 + 164, PKS 1127 – 145, S5 0836 + 710 and PKS 1830 – 211 show the presence of an intervening absorption system along the line of sight, but only the last is known to be gravitationally lensed. AO 0235 + 164 was detected during an outburst and its SED shows a clear shift of the synchrotron peak. 3C 273 shows a change in state with respect to the previous *BeppoSAX* observations that can be interpreted as an increase of the Seyfert-like component and a corresponding decline of the jet emission. This is consistent with the monitoring at radio wavelengths performed during the same period. PKS 1406 – 706 is detected with a flux higher than in the past, but with a corresponding low optical flux. Although it is classified as FSRQ, the SED can be modelled with a simple synchrotron self-Compton model.

Key words. Galaxies: active – BL Lacertae objects: general – Quasars: general – X-rays: galaxies

1. Introduction

There is general consensus on the supermassive black hole (SMBH) paradigm as the central engine of active galactic nuclei (AGN). It is more difficult to obtain quantitative understanding of the physical mechanisms responsible for the observed properties of these cosmic sources. In the AGN zoo, γ–ray loud objects – where with this term we consider the AGN detected at $E >$ 100 MeV – represent a small, but interesting class. Their discovery dates back to the start of γ–ray astronomy, when the European satellite *COS-B* (1975 – 1982) detected photons in the 50 – 500 MeV range from 3C273 (Swanenburg et al. 1978). However, 3C273 remained the only AGN detected by *COS-B*. A breakthrough in this research field came later with the Energetic Gamma Ray Experiment Telescope (EGRET) on board the *Compton Gamma-Ray Observatory* (*CGRO*, 1991-2000). The third catalog of point sources contains 271 sources detected at energies greater than 100 MeV: 93 of them are identified with blazars (66 at high confidence and 27 at low confidence), and 1 with the nearby radiogalaxy Centaurus A (Hartman et al. 1999). Among the remaining sources, there are 5 pulsars, the Large Magellanic Cloud, one exceptional solar flare, and 170 are unidentified. Therefore, EGRET discovered that the blazar-type AGN are the primary source of the extragalactic background in the MeV-GeV range, as suggested by several authors (e.g. Strong et al. 2004, Giommi et al. 2006).

Send offprint requests to: foschini@iasfbo.inaf.it (L. Foschini).

⋆ Based on public observations obtained with *XMM–Newton*, an ESA science mission with instruments and contributions directly funded by ESA Member States and the USA (NASA).

Table 1. Main characteristics of the observed AGN. Columns: (1) Name of the source from the Third EGRET Catalog; (2) Name of the known counterpart; (3) Other name; (4) classification of the active nucleus (LBL: low frequency peaked BL Lacertae Object; HBL: high frequency peaked BL Lacertae Object; FSRQ: flat-spectrum radio quasar; RG: radio galaxy); (5) Coordinates (J2000); (6) Redshift; (7) Galactic absorption column density [10^{20} cm^{-2}] from Dickey & Lockman (1990).

3EG	Counterpart	Other Name	AGN Type	α,δ	z	$N_{\rm H}$
(1)	(2)	(3)	(4)	(5)	(6)	(7)
J0222 + 4253	0219 + 428	3C 66A	LBL	02 : 22 : 39.6,+43 : 02 : 08	0.444	8.99
J0237 + 1635	AO 0235 + 164		LBL	02 : 38 : 38.9,+16 : 36 : 59	0.94	8.95
J0530 − 3626	PKS 0521 − 365		FSRQ	05 : 22 : 58.0,−36 : 27 : 31	0.05534	3.33
J0721 + 7120	S5 0716 + 714		LBL	07 : 21 : 53.4,+71 : 20 : 36	$> 0.5^{*}$	3.81
J0845 + 7049	S5 0836 + 710	4C 71.07	FSRQ	08 : 41 : 24.3,+70 : 53 : 42	2.172	2.91
J1104 + 3809	Mkn 421		HBL	11 : 04 : 27.3,+38 : 12 : 32	0.03002	1.38
J1134 − 1530	PKS 1127 − 145		FSRQ	11 : 30 : 07.0,−14 : 49 : 27	1.184	4.02
J1222 + 2841	ON 231	W Comae	LBL	12 : 21 : 31.7,+28 : 13 : 59	0.102	1.88
J1229 + 0210	3C 273		FSRQ	12 : 29 : 06.7,+02 : 03 : 09	0.15834	1.79
J1324 − 4314	Cen A	NGC 5128	RG	13 : 25 : 27.6,−43 : 01 : 09	0.00182^{**}	8.62
J1339 − 1419	PKS 1334 − 127		FSRQ	13 : 37 : 39.8,−12 : 57 : 25	0.539	4.82
J1409 − 0745	PKS 1406 − 076		FSRQ	14 : 08 : 56.5,−07 : 52 : 27	1.494	2.77
J1621 + 8203	NGC 6251		RG	16 : 32 : 32.0,+82 : 32 : 16	0.0247	5.47
J1832 − 2110	PKS 1830 − 211		FSRQ	18 : 33 : 39.9,−21 : 03 : 40	2.507	21.9
J2158 − 3023	PKS 2155 − 304		HBL	21 : 58 : 52.0,−30 : 13 : 32	0.116	1.69

* Lower limit evaluated on the basis of the non-detection of the host galaxy (Sbarufatti et al. 2005).
** This redshift is not indicative and the distance of 3.84 Mpc is adopted here. See Evans et al. (2004) for more details.

During the years following these discoveries, much effort has been dedicated to the identification of the remaining 170 sources. This is a challenging enterprise given the large position error contours of EGRET sources (typically $\sim 0^{\circ}.5 - 1^{\circ}$). A significant advancement has been obtained by Sowards-Emmerd et al. (2003, 2004), who performed a radio survey at 8.4 GHz. By using a "figure of merit" obtained combining the 8.4 GHz flux, the radio spectral index and the X-ray flux (when available), they proposed 20 new identifications of EGRET sources with blazar-type AGN. A strong improvement in the identification and discovery of new γ−ray loud AGN is expected with the forthcoming missions *GLAST*[1] and *AGILE*[2].

An important complement to these discoveries was the observations performed by the Italian-Dutch satellite *BeppoSAX* (1996-2002) and operating in the 0.1 − 300 keV energy band (see Ghisellini 2004 for a review on blazar observations with this satellite). During its lifetime, *BeppoSAX* observed more than 80 blazars (Giommi et al. 2002, Donato et al. 2005) and sampled with high sensitivity the X-ray region of the spectral energy distribution (SED) over more than three decades in energy.

The observations of these and other high-energy satellites, together with ground telescopes, led to the discovery that the spectral energy distribution (SED) of blazars is typically composed of two peaks, one due to synchrotron emission and the other to inverse Compton radiation, the latter discovered by *CGRO*/EGRET (von Montigny et al. 1995). Maraschi et al. (1995b) and Sambruna et al. (1996) noted that the broad-band spectra of BL Lac and Flat-Spectrum Radio Quasars (FSRQ) share common features and properties (that justified the common designation of "blazars" proposed by Spiegel in 1978). Fossati et al. (1998) and Ghisellini et al. (1998) proposed a unified scheme where the blazars are inserted into a "sequence" according to their physical characteristics. Low luminosity BL Lac have the synchrotron peak in the UV-soft X-ray energy band and therefore are "high-energy peaked" (HBL). As the synchrotron peak shifts to low energies (near infrared, "low-energy peaked" BL Lac or LBL), the luminosity increases and the X-ray emission can be due to synchrotron or inverse Compton or a mixture of both. In the case of FSRQ, the blazars with the highest luminosity, the synchrotron peak is in the far infrared and the X-ray emission is due to inverse Compton radiation. However, other authors reported failures in the above mentioned scheme (see, for example, Padovani et al. 2003, Landt et al. 2006).

The two-peak SED is a dynamic picture of the blazar behaviour: indeed, these AGN are characterized by strong flares during which the SED can change dramatically (e.g. Tagliaferri et al. 2002). The most striking example of such a behaviour is represented by Mkn 501 – although at γ−ray energies this source was not detected by EGRET, but by TeV telescopes – that during an outburst in 1997 showed a shift of the synchrotron peak to the hard X-ray energy band (50 – 100 keV, Pian et al. 1998). The variability on different time scales and, particularly, the intraday variability, is one of the striking characteristics of blazars and is considered one of the proofs that the continuum is generated by a relativistic jet with a small observing angle (for a review see Wagner & Witzel 1995, Ulrich et al. 1997).

[1] http://www-glast.stanford.edu
[2] http://agile.iasf-milano.inaf.it

XMM-Newton (launched in Dec. 1999, Jansen et al. 2001) is a satellite with the current largest collecting area, useful for timing studies, together with a good sensitivity and spectral resolution. *XMM-Newton* covers a lower frequency range than *BeppoSAX*, i.e. from the optical/UV domain to the X-rays, up to 10 keV. From the large *XMM-Newton* public archive, we have selected and analyzed all the publicly available EGRET-detected AGN data. Although the single observations were originally intended for other purposes, it was possible to carry out a homogeneous analysis and to study the main spectral characteristics of these sources in the X-ray energy band. Several sources of the present sample deserve particular attention and many detailed studies have been published on the individual sources. However, the aim of the present work is to perform an overall view and comparison with previous surveys to search for common features that could explain the $\gamma-$ray generation. Some early resuls of the present work have been presented in Foschini et al. (2006).

This paper is organized as follows: in Sect. 2 the selection criteria, biases and the parameters used in the data analysis are presented; in Sect. 3, the spectral characteristics are shown and compared with other catalogs. The absorption systems are discussed in Sect. 4, and a short note on the X-ray spectral features is presented in Sect. 5. The spectral energy distributions and the blazar sequence is shown in Sect. 6. Sect. 7 contains final remarks. In Appendix A we provide the notes on the individual sources together with the fits and some tabular material.

The cosmology values adopted through the paper, when not explicitly declared, are $H_0 = 70$ km·s^{-1}Mpc^{-1}, $\Omega_\lambda = 0.7$ and $\Omega_\mathrm{m} = 0.3$.

2. Sample selection and data analysis

The starting sample consists of all the AGN in the Third EGRET Catalog (Hartman et al. 1999) updated with the recent results by Sowards-Emmerd et al. (2003, 2004). This sample has been cross-correlated with the public observations available in the *XMM-Newton* Science Archive[3] to search for spatial coincidences in the field of view (FOV) of the EPIC camera, within 10′ of the boresight[4]. 15 AGN have been found (Table 1) as of January 4$^{\mathrm{th}}$, 2006, and for three of them there are more than 5 observations available (see the observation log in Table A.1), making it possible also to study the long term behaviour.

2.1. Biases and caveats

The present work suffers from several biases, but nevertheless it is possible to obtain useful information about the overall behaviour of the $\gamma-$ray loud AGN.

The first source of bias is the Third EGRET catalog itself: the large point spread function (PSF) of the EGRET telescope and its moderate sensitivity, changes in the position from the 2EG to the 3EG catalog, double (or more?) sources not resolved by the EGRET PSF (see the notes on the single sources). Sowards-Emmerd et al. (2005) called for the release of a Fourth EGRET catalog, but a major advancement will be possible when the *GLAST* satellite is operational. The arcminute-sized PSF of the LAT telescope and the higher sensitivity would then improve the confidence of the suggested associations (e.g. 3EG J0530 − 3626 or 3EG J1621 + 8203) or disentangle the multiple contributions of certain EGRET sources (see, for example, 3EG J0222 + 4253).

The use of the *XMM-Newton* public data introduces new biases. Exposures and instrument modes were not selected for a survey, but with completely different purposes (e.g. calibration, ToO, ...). In the *XMM-Newton* archive there are many more pointings than the 46 reported here: some were discarded because of problems in the processing of the observation data files (ODF), some others were not used because the instrument mode does not match the major part of the pointing of the same source[5], or because the observations were still covered by the PI proprietary data rights at the time when the archive was scanned. In spite of 46 observations, the present sample is made of only 15 AGN. Three sources dominate: 3C 273 with 15 observations, PKS 2155 − 304 with 9, and Mkn 421 with 6 (see the observation log in Table A.1).

The large differences in settings of the instrument modes between the individual observations had a particularly severe impact on the OM data (Table A.7). It is not possible to have one single filter to be used as a reference for all the observations. In the best case, the magnitudes with filter UVW1 are available for 18 of 46 pointings. In one case only (PKS 1830 − 211), the optical counterpart of the blazar has a V magnitude ≈ 25 (Courbin et al. 2002) and therefore is beyond the instrument capabilities.

2.2. Common procedures of data analysis

For the processing, screening, and analysis of the data from the EPIC MOS1, MOS2 (Turner et al. 2001) and PN cameras (Strüder et al. 2001), standard tools have been used (`XMM SAS v. 6.1.0` and `HEAsoft v 6.0`). The standard procedures described in Snowden et al. (2004) were followed. Only single pixel events have been selected, excluding border pixels or columns with higher

[3] `http://xmm.vilspa.esa.es/external/xmm_data_acc/xsa/index.shtml`

[4] This maximum distance has been selected to take into account that within that region the telescope vignetting is well corrected according to Kirsch (2005).

[5] This is the case of Mkn 421, 3C 273, and PKS 2155-304, that are calibration sources. For the purposes of the present work, only the pointings with the PN detector in small window mode were used.

Table 2. Best fit model parameters for the 15 AGN (present work). In the case of sources with multiple pointings, the weighted averages are shown. Since PKS 2155 − 304 (3EG J2158 − 3023) is best fitted in 4 pointings with the broken power law model and in the remaining 5 with the simple power law model; we reported the averages of both models. Columns: (1) Name of the source; (2) absorbing column density [10^{20} cm^{-2}]; (3) photon index Γ, if the best fit is a simple power law model or soft photon index Γ_1, if the best fit model is a broken power law; (4) hard photon index Γ_2 for the broken power law model; (5) Break energy [keV].

Name	$N_{\rm H}$	Γ/Γ_1	Γ_2	$E_{\rm break}$
(1)	(2)	(3)	(4)	(5)
0219 + 428	Gal.	$2.91^{+0.12}_{-0.08}$	$2.23^{+0.10}_{-0.09}$	1.3 ± 0.2
AO 0235 + 164	Gal.	2.33 ± 0.04	2.1 ± 0.1	$3.3^{+0.7}_{-0.5}$
PKS 0521 − 365	Gal.	1.95 ± 0.03	1.74 ± 0.03	$1.5^{+0.3}_{-0.2}$
S5 0716 + 714	Gal.	2.70 ± 0.02	$1.98^{+0.08}_{-0.09}$	$2.3^{+0.2}_{-0.1}$
S5 0836 + 710	14 ± 3	1.379 ± 0.007	–	–
Mkn 421	Gal.	2.38 ± 0.09	2.7 ± 0.2	2.7 ± 1.0
PKS 1127 − 145	12^{+2}_{-1}	$1.40^{+0.08}_{-0.05}$	1.22 ± 0.06	$2.7^{+1.0}_{-0.8}$
ON 231	2.5 ± 0.6	2.77 ± 0.04	–	–
3C 273	Gal.	2.02 ± 0.08	1.67 ± 0.05	1.44 ± 0.08
Cen A	1523 ± 261	2.22 ± 0.06	–	–
PKS 1334 − 127	6.7 ± 0.9	1.80 ± 0.04	–	–
PKS 1406 − 076	Gal.	1.59 ± 0.01	–	–
NGC 6251	14 ± 1	$2.11^{+0.08}_{-0.06}$	1.78 ± 0.07	$2.5^{+0.3}_{-0.4}$
PKS 1830 − 211	63 ± 1	1.00 ± 0.09	1.32 ± 0.06	3.5 ± 0.7
PKS 2155 − 304	1.69 ± 0.06	2.9 ± 0.1	–	–
	Gal.	2.7 ± 0.1	2.94 ± 0.06	2.7 ± 0.7

Table 3. Best fit model parameters for the 15 AGN from the *BeppoSAX* catalogs by Giommi et al. (2002) and Donato et al. (2005). The values are the weighted averages obtained from multiple observations (if any) and from the two catalogs. In the case of 3C 273 (3EG J1229 − 0210) there were 9 observations, 5 best fitted with a broken power law and 4 with a single power law model: both model averages are reported. For NGC 6251 (3EG J1621 + 8203) the average is obtained from Chiaberge et al. (2003) and Guainazzi et al. (2003) from a fit in the energy band 0.1 − 200 keV. Grandi et al. (2003) is the reference for Cen A (3EG J1324 − 4314), from a fit in the energy band 0.4 − 250 keV excluding the 5.5 − 7.5 keV band (iron emission line). The value for PKS 1830 − 211 (3EG J1832 − 2110) has been obtained by De Rosa et al. (2005) from a fit in the energy band 0.5 − 80 keV (*Chandra* and *INTEGRAL*). Columns: (1) Name of the source; (2) absorbing column density [10^{20} cm^{-2}]; (3) photon index Γ, if the best fit is a simple power law model or soft photon index Γ_1, if the best fit model is a broken power law; (4) hard photon index Γ_2 for the broken power law model; (5) Break energy [keV].

Name	$N_{\rm H}$	Γ/Γ_1	Γ_2	$E_{\rm break}$
(1)	(2)	(3)	(4)	(5)
0219 + 428	Gal.	2.22 ± 0.06	–	–
AO 0235 + 164	Gal.	2.0 ± 0.1	–	–
PKS 0521 − 365	Gal.	1.74 ± 0.02	–	–
S5 0716 + 714	Gal.	2.5 ± 0.2	1.8 ± 0.1	3.0 ± 0.4
S5 0836 + 710	78^{+55}_{-35}	1.31 ± 0.02	–	–
Mkn 421	Gal.	1.9 ± 0.2	2.3 ± 0.3	1.3 ± 0.8
PKS 1127 − 145	Gal.	1.42 ± 0.05	–	–
ON 231	Gal.	2.58 ± 0.01	1.52 ± 0.06	2.8 ± 0.2
3C 273	Gal.	2.0 ± 0.1	1.603 ± 0.006	0.9 ± 0.3
	Gal.	1.58 ± 0.03	–	–
Cen A	1020^{+90}_{-40}	$1.80^{+0.03}_{-0.04}$	–	–
PKS 1334 − 127	–	–	–	–
PKS 1406 − 076	–	–	–	–
NGC 6251	9 ± 1	1.79 ± 0.06	–	–
PKS 1830 − 211	194^{+28}_{-25}	1.09 ± 0.05	–	–
PKS 2155 − 304	Gal.	2.3 ± 0.1	2.8 ± 0.1	1.7 ± 0.2

offset. High-background flares affected the observations randomly, and in some cases it was necessary to filter the available data. Time intervals contaminated by flares have been excluded by extracting the whole detector lightcurve for $E > 10$ keV and by removing the periods with count rates higher than 1.0 s^{-1} for PN and 0.35 s^{-1} for MOS, as suggested by Kirsh (2005).

The source spectra have been extracted from a circular region with a radius of 40″ and centered in the catalog (radio) position of the AGN. The background to be subtracted in the analysis was derived from a circular region, with the same radius, near the selected source. In the case of pile-up, the source region is an annulus with still an external radius of 40″ and an internal radius selected to minimize the pile-up effects by using the task `epatplot` of `XMM SAS`. It resulted 8″ for 3C 273 and PKS 2155 – 304, and 10″ for Mkn 421. For Cen A, the annulus has internal and external radii of size 20″ and 50″, respectively.

Since PN is the most stable detector, with negligible degradation of performance to date, we adopted it as the prime instrument. Data from MOS cameras have been used only when it was necessary to check a finding obtained with the PN detector or to increase the statistics of a specific observation. For very bright sources (with fluxes of the order of 10^{-10} erg cm^{-2} s^{-1} or more), only the PN data in small window mode have been analyzed.

The spectra were rebinned so that each energy bin contained a minimum of 20 counts and fit in the 0.4 – 10 keV energy range for the PN detector and 0.5 – 10 keV for MOS detectors, because of the uncertainties in the calibration and cross-calibration at lower energies (cf. Kirsch 2005). The fluxes and luminosities were calculated in the 0.4 – 10 keV band by extrapolating the model spectrum with the command `extend` of `xspec`. The photon redistribution matrix and the related ancillary files were created appropriately with the `rmfgen` and `arfgen` tasks of `XMM-SAS`.

The data from the Optical Monitor (Mason et al. 2001) were also reprocessed with the latest version of `SAS`.

Through the paper, we report only the fits with reduced χ^2 less than 2 ($\tilde{\chi}^2 < 2$) and we consider significant improvement in the fit with $Ftest > 99\%$. In the case of an *added* spectral component, we evaluated the improvement of the fit by the $\Delta\chi^2$ value (cf Protassov et al. 2002). All the quoted uncertainties in the parameters are at the 90% confidence level for 1 parameter ($\Delta\chi^2 = 2.71$), unless otherwise stated.

3. Average spectra and comparisons with other catalogs

Most of the sources analyzed here are blazars, except for two radiogalaxies Fanaroff-Riley Type I (FRI), that are thought to be blazar-like sources seen at large viewing angles (Urry & Padovani 1995). Blazars display featureless X-ray continuum, occasionally with hints of breaks, curvature, or, more seldom, a soft excess (e.g. Giommi et al. 2002, Donato et al. 2005, Perlman et al. 2005). Radiogalaxies can have a much more complex environment at low energies (e.g. Evans et al. 2005, Grandi et al. 2005). However, since the main purpose of this work is to study and compare the continuum properties, we decided to fit the X-ray spectra with a redshifted power-law model (`zpo` in `xspec`; see Table A.2) and a broken power law model (`bknpo` in `xspec`; see Table A.3). The absorption can be fixed to the Galactic column density (Dickey & Lockman 1990) or fitted. Sometimes a more complex fit is necessary and is analyzed separately. More details on the fits are available in Appendix A (tables and notes on the individual sources).

Several of the 15 sources analyzed here show significant variability, particularly on small time scales. Therefore, the comparison of average spectral parameters presented here (Table 2) and the values available in the *BeppoSAX* catalogues by Giommi et al. (2002) and Donato et al. (2005), can be considered a indicator of long term spectral variability, since *XMM-Newton* observations refer to the period 2000 – 2004 and *BeppoSAX* data have been collected in the period 1996 – 2002. The spectra of the present work are generally best fitted with broken power law models (9/14 in Table 2 without PKS 2155 – 304, that is fitted with both models), compared to only 4/14 sources in *BeppoSAX* data (Table 3, without 3C 273, that is fitted with both models). There is a possible important bias factor in *BeppoSAX* fits. The Italian-Dutch satellite concentrators LECS and MECS have energy bands overlapping at ≈ 2 keV, where most of the blazars have the break energy. Therefore, it is also possible that – in some cases – the intercalibration constant between the two detectors could have "absorbed" some spectral shape variations, thus leading to prefer the single power law model. This could be the case of PKS 1127 – 145, that is known to have an intervening system along the line of sight, but the *BeppoSAX* fit does not require an additional absorption.

In other cases, there are changes in the source state (e.g. AO 0235+164, that in the present observation was found in outburst) or 3C 273, as already noted by Page et al. (2004). In the latter case, the blazar shows in the *XMM-Newton* data an increase of the break energy and a small softening of Γ_2, the photon index at $E > E_{\rm break}$. Also Cen A shows a softer photon index and a flux lower by a factor of 4 with respect to the *BeppoSAX* data analyzed in Grandi et al. (2003). In the two HBL (Mkn 421 and PKS 2155 – 304), the broken power law model appears to be the simplification of a more complex curved model, as already noted by Brinkmann et al. (2001, 2003), Sembay et al. (2002), Ravasio et al. (2004).

Comparing the parameters in Table 2 with the larger catalogs by Giommi et al. (2002), Donato et al. (2005), Evans et al. (2005), Grandi et al. (2005) containing also radio-loud AGN not detected by EGRET, there are no signs of differences between $\gamma-$ray loud and quiet AGN.

The analysis of the three most intensively observed sources is in agreement with the typical behaviour of these types of sources. Even though they require a broken power law model, to have an overall view of the source behaviour, we correlate the photon index of the single power law model with its normalization at 1 keV. This gives an idea of the behaviour of the spectral shape with flux variations.

PKS 2155 – 304 shows a clear correlation (linear correlation coefficient $r = -0.76$ for 8 observations and $p \leq 0.035$), with a hardening of the photon index with increasing flux (Fig. 1, *bottom right*) if one point is not considered (ObsID 0124930301). While the behaviour of most points can be explained by considering a flux increase with a constant synchrotron peak (implying

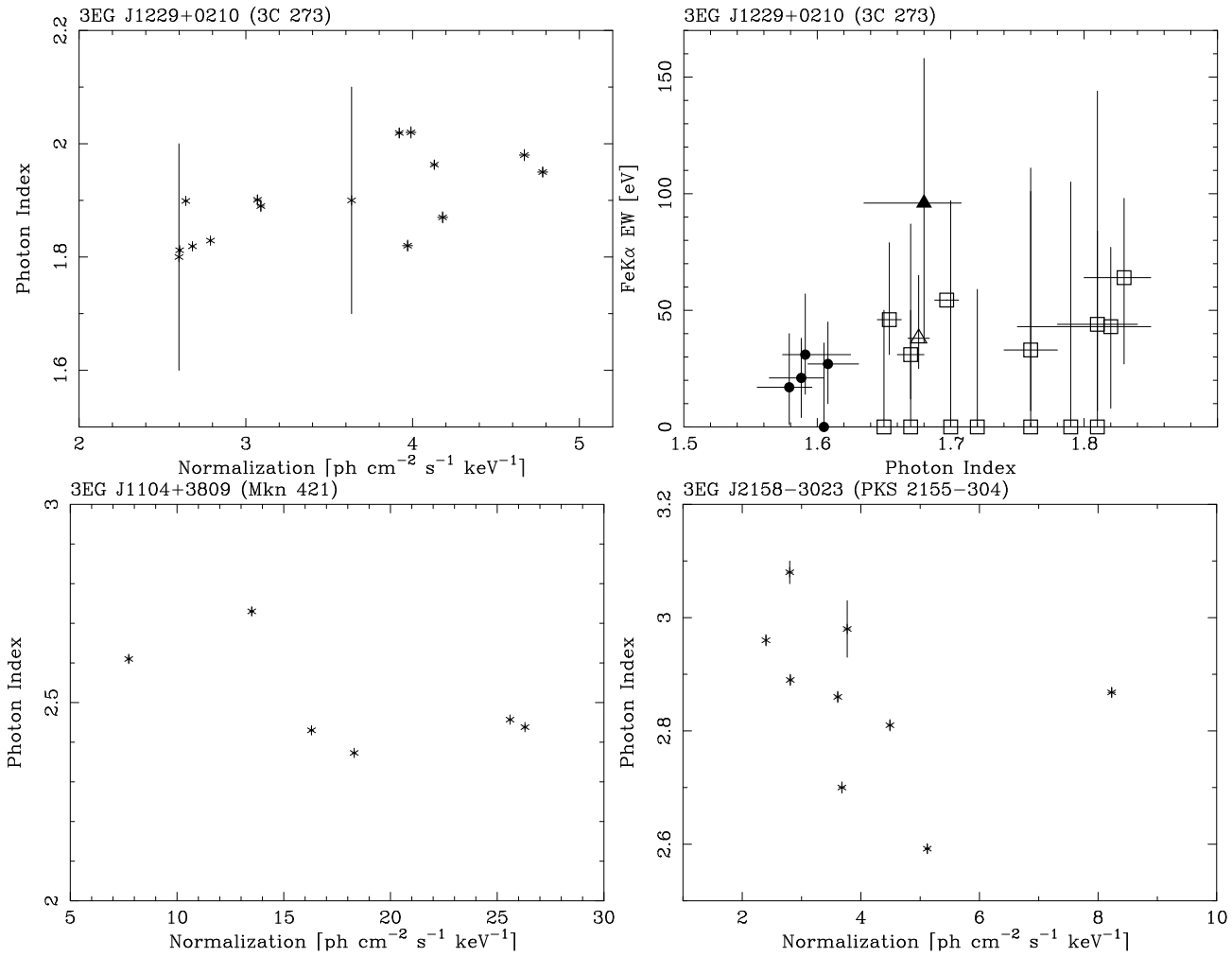

Fig. 1. Correlations: Photon index versus normalization for (*top left*) 3C 273 (3EG J1229 + 0210), (*bottom left*) Mkn 421 (3EG J1104 + 3809), and (*bottom right*) PKS 2155 − 304 (3EG J2158 − 3023). (*top right*) Equivalent width of the FeKα line versus photon index for 3C273. The open square indicates the *XMM-Newton* data from the present work, while the filled circle represents the values from *BeppoSAX* observations reported in Grandi & Palumbo (2004). The points of the simultaneous *BeppoSAX*-*XMM-Newton* observation (June 2001) are tagged with a triangle, filled for *BeppoSAX* and open for *XMM-Newton*.

a hardening of the spectrum), the outlying point can be explained as due to a frequency shift of the synchrotron peak. For this ObsID, OM data (Table A.7) suggest a high flux level in the bands U, B, and V, but, again, available magnitudes are fragmentary and it is not possible to search for more stringent correlations.

The correlation in Mkn 421 is poor ($r = -0.60$ for 6 points, $p \leq 0.2$), although a general trend of spectral hardening with flux increasing can be noted (Fig. 1, *bottom left*).

3C 273 shows instead a spectral softening with flux increasing (Fig. 1, *top left*, $r = 0.66$ with 15 observations, $p \leq 0.0077$), although there is a non negligible scatter of the points, suggesting that other processes are playing important roles in this sources. Indeed, it is known that this blazar also has a Seyfert-like component that can be detected (Grandi & Palumbo 2004). Fig. 1 (*top right*) shows the equivalent width of the FeKα line versus the photon index for both *BeppoSAX* observations (filled circles; data from Grandi & Palumbo 2004) and the present work (open squares; for *XMM-Newton* see Table A.5). 3C 273 was in a different state during the two satellites observations with only one point overlapping, when using the simultaneous *BeppoSAX* and *XMM-Newton* observation performed in June 2001 (ObsID 0136550101, triangles in Fig. 1 *top right*) to cross-calibrate the respective instruments (cf Molendi & Sembay 2003). This strenghtens the validity of the other values obtained by the two satellites as indicating an effective change in the state of the source. The general trend can be understood, in the framework of the Grandi & Palumbo (2004) results on 3C 273 and the more general picture on blazars outlined by Maraschi & Tavecchio (2003), as a weakening of the jet component and an increase of the Seyfert-like part. With respect to the *BeppoSAX* observations (1996 – 2002), we noted in the *XMM-Newton* observations (2000 – 2004), an increase of the "thermal" component and a softening of the hard photon index The former is indicated in the broken power law model by a shift to high energies of the break energy

(see Table 2: the average value for *XMM-Newton* is $E_{\rm break} = 1.44 \pm 0.08$ keV compared to the *BeppoSAX* value of 0.9 ± 0.3 keV); in the blackbody plus power law model (Table A.4) this is indicated by an increase of the temperature (from the average value of 54^{+6}_{-4} eV measured by *BeppoSAX* to 143 ± 6 eV derived from the data analyzed in the present work). This behaviour of the continuum is accompanied by an increase of the equivalent width of the (broad) iron emission line either at 6.4 or 6.7 keV (Fig. 1, *top right*). According to the results in Table A.5, the major improvements in the fit occur with the detection of the (broad) iron line centered at 6.4 or 6.7 keV, but sometimes there is no detection at all. If we consider that the detection and the energy centroid are related to different degrees of ionization (see, for example, the review by Reynolds & Nowak 2003), the interpretation of the data still favours the hypothesis of an increase of the accretion around the SMBH. A more detailed spectral analysis is required to better assess the state variation of 3C 273, but this is outside the scope of the present work. However, the general trend outlined here is also confirmed by the radio data reported, for example, by Teräsranta et al. (2005) with observations at 22 and 37 GHz: there is a decreasing of activity from 1996, with an outburst in 2003, but smaller than in 1998 – 1999.

Another interesting case in the present sample is AO 0235+164, that displays the typical characteristics of blazars in outburst. This should be compared with the negative detection of variability reported in the 2004 observations (Raiteri et al. 2005). A more detailed analysis of all the *XMM-Newton* data sets (both public and private) is available in Raiteri et al. (2006). In the present observation, the source displays a shift of the synchrotron peak (see the discussion in Section 6), with a hint of periodicity of 7829 s (significance 4.5σ), but with a low quality factor, because of a limited number of cycles (2.15). An inspection of the lightcurve suggests that this periodicity is transient: periodic flares appear during the activity phase of the source, while X-ray observations of the source in quiescence have detected constant flux and, obviously, no periodicities (Raiteri et al., 2006).

4. Intervening absorption

Torres et al. (2003) have suggested that gravitational microlensing can boost the $\gamma-$ray flux. Therefore, we searched in the present sample for any presence of intervening systems of any type.

Damped Lyman$-\alpha$ (DLA) systems (see Wolfe et al. 2005 for a review) are present along the line of sight toward AO 0235+164 and PKS 1127−145. In the case of AO 0235+164 ($z = 0.94$, Cohen et al. 1987), the intervening system is placed along the line of sight at $z = 0.524$ (see, e.g., Raiteri et al. 2005 for a more recent discussion on this). This intervening system has been measured by *ROSAT* and *ASCA* obtaining a value of $N_{\rm H}^z = (2.8 \pm 0.4) \times 10^{21}$ cm^{-2} (Madejski et al., 1996). In addition, Raiteri et al. (2005) measured a value of $N_{\rm H}^z = (2.4 \pm 0.2) \times 10^{21}$ cm^{-2} with an *XMM-Newton* observation performed on January 18, 2004. The present spectrum in the $0.4 - 10$ keV energy band for PN and the $0.5 - 10$ keV band for the two MOS detectors is the best fit with a broken power law model absorbed by the Galactic column together with one at redshift $z = 0.524$ with $N_{\rm H}^z = (2.56 \pm 0.05) \times 10^{21}$ cm^{-2}. The low energy photon index is $\Gamma_1 = 2.50 \pm 0.01$ and the high-energy one is $\Gamma_2 = 2.05 \pm 0.03$, with the break at $3.08^{+0.09}_{-0.12}$ keV, for a $\tilde{\chi}^2 = 1.10$ and 801 dof (see also Appendix A).

PKS 1127 − 145 is another quasar with an additional absorber at $z = 0.321$ along the line of sight, probably due to two late-type galaxies (Bergeron & Boissé 1991, Lane et al. 1998). The best fit model is the broken power law, with the $z = 0.321$ absorption column of $(1.2^{+0.2}_{-0.1}) \times 10^{21}$ cm^{-2}, the Galactic column, and no intrinsic absorption. *Chandra* observations reported the same absorption, but the continuum is best fitted with a single power law with $\Gamma = 1.19 \pm 0.02$ (Bechtold et al. 2001).

The absorption in X-rays, in both the above cases, is lower than that measured from optical observations, but it can be due to different metallicity ($Z < Z_\odot$) or to the presence of dust with a ratio different from that in the Galaxy, that is common in DLA systems (Pei et al. 1991, Pettini et al. 1994). However, what is important in these systems is the presence of galaxies along the line of sight that can cause gravitational lensing effects, which in turn enhance the flux of the background blazar.

Another blazar (S5 0836+710) presents an intervening system at $z = 0.914$, but optical observations by Stickel & Kühr (1993) indicated the presence of Mg II $\lambda\lambda 2796, 2803$, which do not qualify this system as damped Lyman$-\alpha$. The blazar spectrum, already quite hard, presents a spectral flattening at low energies. This type of flattening has been observed in other blazars at high redshift ($z > 2$; see, e.g., PMN J0525 − 3343 in Fabian et al. 2001 or on RBS 315 in Piconcelli & Guainazzi 2005) and a few hypotheses have been invoked, like instrinsic absorption or intrinsic spectral properties. The best fit for S5 0836 + 710 is that with the additional absorption at the redshift of the quasar and no improvements are obtained by adding an absorber at the redshift of the intervening system ($z = 0.914$). Therefore, it appears that this system is not responsible for the additional absorption or – at least – the present data do not allow us to separate the different components, if any. Radio observations by Hutchison et al. (2001) show that near the blazar core the polarization is very low with respect to typical values in other quasars. The authors explained this by the presence of an external environment surrounding the jet (a cocoon?). Such a plasma cocoon could act like the "warm absorber" of Seyferts and explain the spectral flattening at low energies. Yet another hypothesis is a low-energy cut-off in the relativistic electron distribution at $\gamma_{\rm min}$, which would yield a flattening below $\approx \gamma_{\rm min}^2 \Gamma^2 \nu_{\rm ext}$, where $\nu_{\rm ext}$ is the peak frequency of the seed photon radiation field. These hypotheses are discussed in, e.g., Fabian et al. (2001).

Two more sources in the present sample show evidence of intrinsic absorption and are the two radiogalaxies (Cen A and NGC 6251). This is known to be due to the environment in the radiogalaxies (cf Evans et al. 2005, Grandi et al. 2005).

The last case of intervening systems is PKS 1830 − 211 ($z = 2.507$), that is gravitationally lensed by a galaxy at $z = 0.886$ found by Wiklind & Combes (1996) through infrared observations of hydrocarbon absorption lines. The fit with a redshifted power law model absorbed by the Galactic column and the intervening system at $z = 0.886$, gives results consistent with previous

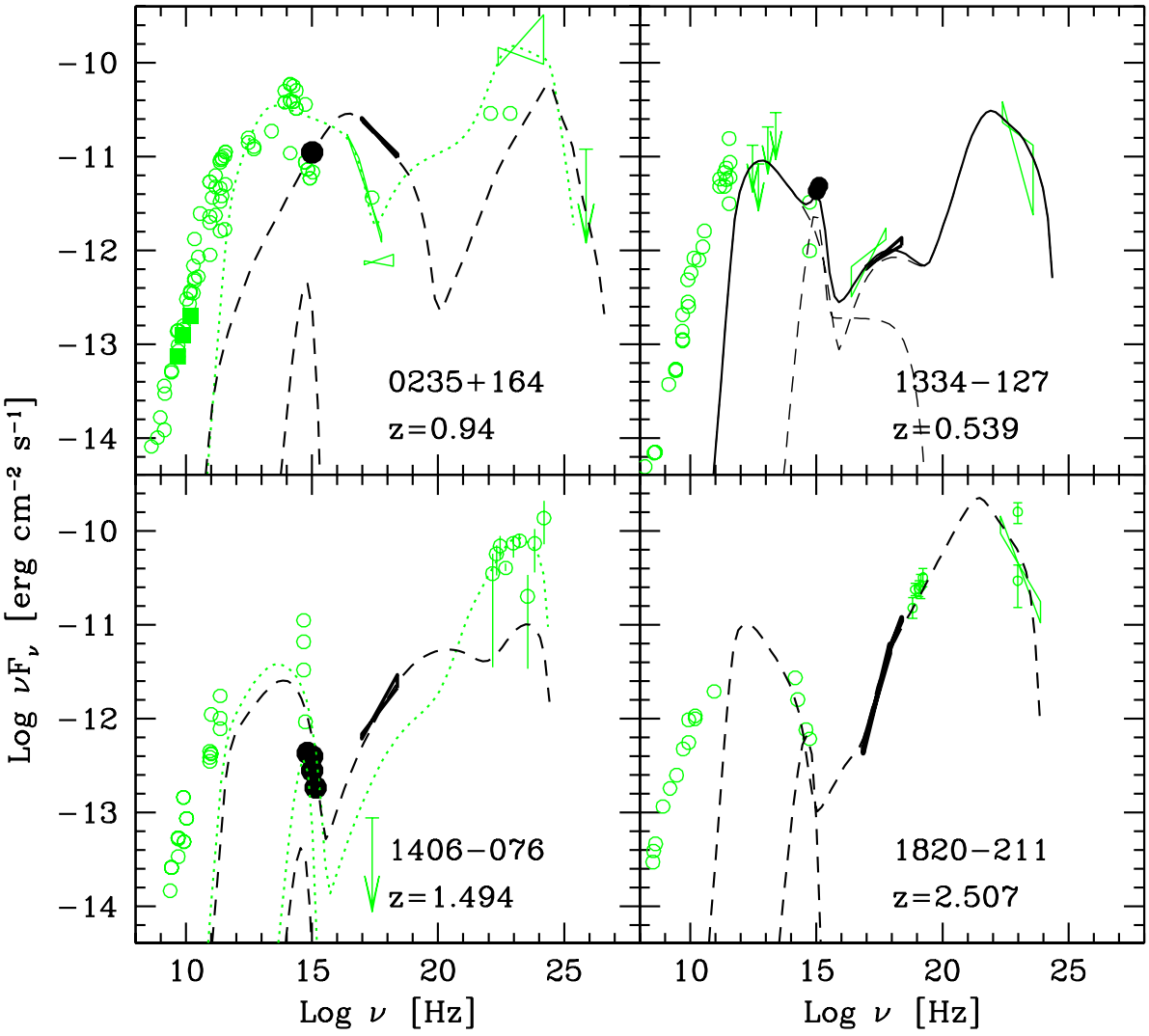

Fig. 2. SED of newly modelled blazars: (*top*, *left*) AO 0235 + 164; (*top*, *right*) PKS 1334 – 127; (*bottom*, *left*) PKS 1406 – 076; (*bottom*, *right*) PKS 1830 – 211, not corrected for the gravitational lensing effects. The black line is a single–zone synchrotron inverse Compton model using the input parameters listed in Table 4. In all the SED, the *XMM–Newton* data are indicated with black filled symbols, while the remaining symbols and lines (grey) refer to archival data. The bump at $\sim 10^{14-15}$ Hz is the assumed disk spectrum.

X-ray analyses by Mathur & Nair (1997), Oshima et al. (2001), and De Rosa et al. (2005). The absorption due to the intervening system averaged over the three observations is $N_{\rm H}^{\rm z} = (2.3 \pm 0.1) \times 10^{22}$ cm^{-2} and the photon index is $\Gamma = 1.14 \pm 0.02$. However, some residuals at low energy are present and an improvement in the fit (with $\Delta\chi^2 = 30.9$, 103, and 16.6 for a decrease of two degrees of freedom, for the three observations respectively) can be obtained by adding a thermal plasma model (`mekal`) at the redshift of the blazar, with solar abundances and temperature $kT = 0.39 \pm 0.06$ keV. The absorption of the intervening system is slightly greater ($N_{\rm H}^{\rm z} = (3.0 \pm 0.4) \times 10^{22}$ cm^{-2}) and the photon index a little steeper ($\Gamma = 1.21 \pm 0.04$). This thermal plasma can be the "warm absorber" suggested by Fabian et al. (2001) to explain the X-ray deficit at low energies in high redshift blazars. Interestingly, the statistical best fit of these three *XMM-Newton* observations is obtained with a broken power law model and lower absorption (Table A.3), thus suggesting that the low X-ray deficit could be due to something intrisic to the electron distribution.

Table 4. Parameters for the models of AO 0235 + 164, PKS 1334 − 127, PKS 1406 − 076, and PKS 1830 − 211: above the dividing line are listed the input parameters used to model the SED according to the finite injection time synchrotron–inverse Compton model of Ghisellini, Celotti & Costamante (2002). Below the dividing line we list the output parameters for the four fitted sources. See the text for more details.

Parameter	AO 0235 + 164	PKS 1334 − 127	PKS 1406 − 076	PKS 1830 − 211	Units
R	4.5	3.5	2.0	2.0	10^{16} cm
ΔR	2.8	3.5	2.0	30	10^{15} cm
$L'_{\rm inj}$	7.5	3.0	3.0	7.0	10^{43} erg s^{-1}
$\gamma_{\rm break}$	2.0×10^4	2.5×10^2	1.0×10^2	1.4×10^2	
$\gamma_{\rm max}$	6.0×10^5	4.0×10^3	5.0×10^3	1.6×10^3	
s	2.55	2.7	2.2	2.8	
B	1.3	3.7	1.0	3.8	Gauss
Γ	16	10	10	17	
θ	3	6	3.6	3.5	degree
δ	18.2	9.6	14.3	16.4	
L_{BLR}	3.0	4.5	0.8	12	10^{44} erg s^{-1}
R_{BLR}	7.0	3.5	5.0	3.5	10^{17} cm
$\gamma_{\rm peak}$	2.0×10^4	2.5×10^2	1.6×10^3	1.4×10^2	
U_B	0.067	0.54	0.04	0.57	erg cm^{-3}
$U'_{\rm r}(\gamma_{\rm peak})$	0.042	1.8	0.25	10.87	erg cm^{-3}
L_B	3.28	6.26	0.15	14	10^{45} erg s^{-1}
$L_{\rm e}$	1.05	1.78	8.8	1.0	10^{45} erg s^{-1}
$L_{\rm p}$	7.16	3.15	25	26.5	10^{46} erg s^{-1}
$L_{\rm rad}$	4.588	3.59	3.2	20.8	10^{45} erg s^{-1}

5. X-ray spectral line features

The spectra of the AGN in the present sample sometimes show some features, but these are generally within 2σ deviations from the best fit model. For more significative detections (e.g. in PKS 2155 − 304, known to be due to warm-hot intergalactic medium, see Cagnoni et al. 2004), we bypassed the problem with a proper selection of the energy band, since the study of these features is outside the aims of the present work. No evidence ($> 3\sigma$) of features linked to physical characteristic of any cosmic source is found in the present data set, except for the iron line complex of Cen A (see Table A.6 and the note on this source in Appendix A) and some detections in 3C 273 (Table A.5). The latter is not always evident, although a forced fit with a broad iron line both neutral and ionized can give sometimes a non negligible improvement in the χ^2. The implications have been already discussed in the Sect. 3.

6. Spectral Energy Distributions and the blazar sequence

SED have been constructed and modelled to study the multiwavelength emission over a broad energy range. All but two (PKS 1334 − 127 and PKS 1830 − 211) of the blazars in the present sample have been studied in detail by Ghisellini et al. (1998), Tagliaferri et al. (2000), Ghisellini, Celotti & Costamante (2002). The radiogalaxies have been studied in Chiaberge et al. (2001, 2003), Guainazzi et al. (2003), Foschini et al. (2005), and Ghisellini et al. (2005). We refer to these papers and to the references therein. The SED with *XMM-Newton* data are reported in Fig. A.1 and A.2, together with the model of synchrotron and inverse Compton radiation (including self-Compton and external Compton) in a homogeneous region applied to the data. The results obtained do not change dramatically with respect to the above mentioned works.

There are however four cases, namely AO 0235 + 164, PKS 1334 − 127, PKS 1406 − 76 and PKS 1830 − 211, which are worth investigating further. AO 0235 + 164 shows a clear shift in its peak frequency, as expected during flaring activities of blazars: the present *XMM-Newton* observation was performed when the source was in outburst (see Sect. 3). PKS 1334 − 127 has been associated with an EGRET source only in the Third Catalog (Hartman et al. 1999), and therefore is missing in Ghisellini et al. (1998). PKS 1406 − 076 was never detected in X-rays and PKS 1830 − 211 is a gravitationally lensed system, also missing in Ghisellini et al. (1998).

We therefore applied the same model used in Ghisellini, Celotti & Costamante (2002) in order to find out the physical parameters of the four sources. The main assumptions of the model can be summarized as follows: the geometry of the source is a cylinder – except for PKS 1830 − 211, that is analyzed later – of radius R and length, in the comoving frame, $\Delta R' = R/\Gamma$, where Γ is the bulk Lorentz factor; θ is the viewing angle, δ the Doppler factor, and B the magnetic field. The radiating particle distribution is assumed to be $N(\gamma) \propto \gamma^{-s}$, where the value of s depends on the value of γ of the injected particles. The injected power in the comoving frame is $L'_{\rm inj}$. The external seed photon field has a dimension R_{BLR} and luminosity L_{BLR}. It is assumed to mainly originate in a Broad Line Region or any other external source and it is calculated as a fraction of the disk luminosity

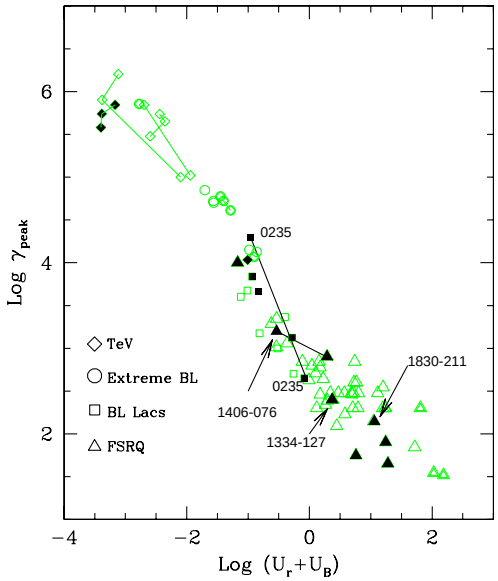

Fig. 3. Updated blazar sequence, adapted from Ghisellini, Celotti & Costamante (2002), with the addition of the new TeV BL Lacs. We mark with black filled symbols the sources analyzed in this paper, emphasizing AO 0235 + 164 (in quiescence and during the outburst presented in this work), PKS 1334 − 127, PKS 1406 − 076 (the fit without the X-ray detection and with the present data), and PKS 1830 − 211.

(generally 10%). The magnetic and radiative energy densities are indicated with U_B and $U_{\rm r}$, respectively. Electron, proton and radiation powers are represented by $L_{\rm e}$, $L_{\rm p}$, and $L_{\rm rad}$, respectively.

Fig. 2 show the model with the SED, while in Table 4 we list the input and output parameters for the model. Only AO 0235 + 164 displays significant variability in the model parameters with respect to Ghisellini et al. (1998), but it continues to fulfill the requirements of the blazar sequence. PKS 1334 − 127 behaves as a typical FSRQ.

The X-ray emission of PKS 1406 − 076 is modelled as due to the inverse Compton emission from synchrotron seed photons, although this source is a FSRQ. An external source of seed photons is needed to generate γ−rays in the EGRET energy band (not simultaneous data) and there is an apparent anti-correlation between X-ray and optical/UV emission: indeed, this first X-ray detection is simultaneous with low optical flux, while archival data (not simultaneous) report higher optical flux and only an upper limit in X-rays (for more details, see the note on this source in the Appendix). This does not allow us to claim an anti-correlation.

In the case of PKS 1830 − 211, there are some problems that should be taken into account: the magnification effects of the gravitational lensing are still uncertain (cf Oshima et al. 2001 and Courbin et al. 2002) and so as the absorption, both due to the Galactic column (the source is apparently located at low Galactic latitude, with Galactic coordinates $l = 12^\circ.16$ and $b = -5^\circ.71$) and to the intervening system. Therefore, instead of making hypotheses about the quantity and quality of corrections to be applied, we decided to analyze the observed SED without any correction. This means that the anomalies in the parameters of PKS 1830 − 211 (Table 4) reflect the uncertainties in the magnification and the absorption. For example, the needed L_{BLR} necessary for the external Compton contribution was calculated as 30% of the disk luminosity, while for the three other blazars a value of 10% was taken. A proper dereddening could result in the needed optical flux, without invoking an increase of percentage of the disk luminosity.

The location of the sources analyzed here in the blazar sequence can be seen in Fig. 3, where we show $\gamma_{\rm peak}$, the Lorentz factor of the electrons radiating mostly at the peak of the SED, versus $U_B + U'_{\rm rad}$, the radiation plus magnetic energy density in the comoving frame. Fig. 3 has been updated by adding 3 new BL Lac recently detected in the TeV range (see Aharonian et al. 2005a, 2005b). These new TeV BL Lacs, namely 1ES 1101 − 232 (cf also Wolter et al. 2000), PKS 2005 − 489, and H 2356 − 309, lie in the "high energy branch" defined by the BL Lacs previously detected in the TeV band. Interestingly, PKS 1406 − 076 moved toward the region of the BL Lac region, while the previous modeling – with only an upper limit in X-rays – placed this FSRQ in the region typical of these sources.

The presence of two radiogalaxies in the present sample suggests some hints about the paradigm of the unification of radio-loud AGN (Urry & Padovani 1995), of which the γ−ray loud AGN are the subclass analyzed in this work. This paradigm and the theories on the blazar evolution (see Böttcher & Dermer 2002, Cavaliere & D'Elia 2002, Maraschi & Tavecchio 2003) find analogies between BL Lac and FRI on one side and FSRQ and FRII on the other. BL Lac and FRI are evolved AGN, with low emission from the environment around the SMBH, while FSRQ and FRII are instead young sources with a rich environment.

Table 5. Parameters useful to understand γ−ray loudness. Columns: (1) Source name; (2) beaming factor δ; (3) observed flux in the 0.4 – 10 keV energy band [erg cm^{-2} s^{-1}]; (4) intrinsic luminosity in the 0.4 – 10 keV energy band [erg s^{-1}]; (5) Confidence of the EGRET detection (high > 95%; low < 95%).

Source	δ	F	L	Conf.
(1)	(2)	(3)	(4)	(5)
3C 273	6.5 – 7	$\approx 10^{-10}$	$\approx 10^{46}$	high
NGC 6251	3.2 – 3.8	$\approx 10^{-12}$	$\approx 10^{43}$	low
PKS 0521 – 365	1.4 – 3	$\approx 10^{-11}$	$\approx 10^{42}$	low
Cen A	1.2 – 1.6	$\approx 10^{-10}$	$\approx 10^{41}$	high

With reference to the γ−ray propagation from the source to the observer, one of the most important factor is the beaming factor δ, that allow high energy photons to escape from the source without disappearing in pair production. From the SED of the γ−ray loud AGN reported in Ghisellini et al. (1998, 2005), Chiaberge et al. (2001, 2003), Foschini et al. (2005), complemented and confirmed by this work, we see that the δ values for almost all the EGRET detected AGN are above 10, with only a few exceptions. 3C 273 with $\delta = 6.5 - 7$ and Cen A with $\delta = 1.2 - 1.6$ are also the only AGN with $\delta < 10$ detected by EGRET with high confidence. PKS 0521 – 365 ($\delta = 1.4 - 3$) and NGC 6251 ($\delta = 3.2 - 3.8$) have low confidence identifications, that should be confirmed. The two δ of the low confidence detections are in between 3C 273 and Cen A, which are instead detected at high confidence level. Therefore, there should be other reasons to explain the EGRET detections. Indeed, three of the four above sources have also the lowest intrinsic luminosities in the present sample (and also among the whole EGRET sample), but not the fluxes (cf Table 5). This implies that the present definition of γ−ray loudness – that it is defined here simply as the detection at $E > 100$ MeV – is still strongly biased by the instrument sensitivity or by the distance of the source.

Moreover, there is another key point still missing in this picture: γ−ray detection of FRII radiogalaxies, that are still completely missing to date even in the list of hypothetical associations.

7. Final remarks

A small sample of AGN γ−ray loud (i.e. detected by the EGRET instrument on board *CGRO*) observed by *XMM-Newton* has been analyzed in a homogeneous way and presented here. The sample is composed of 15 AGN divided into 7 FSRQ, 4 LBL, 2 HBL, and 2 FRI radiogalaxies. All the data were taken from the public archive of *XMM-Newton*: 46 pointings were analyzed, of which 30 are of three sources only (3C 273, Mkn 421, PKS 2155 – 304).

Despite these limitations, some useful inferences can be made. Indeed, with *XMM-Newton* it is possible to perform simultaneous X-ray and optical/UV observations, that can be particularly useful in blazars to place reliable constraints on the synctrotron and inverse Compton peaks in the SED.

The main findings can be summarized as follows: all the blazars obey the sequence suggested by Ghisellini et al. (1998) and Fossati et al. (1998). The only X-ray features found in the present sample are the emission lines of the iron complex in Cen A and in 3C 273. In the case of Cen A, the iron line at 6.4 keV ($\sigma \lesssim 80$ eV) is known to be due to the transmission of radiation along the dust lane warped around Cen A, while in 3C 273, the broad iron line can be associated with the Seyfert-like component.

The comparison with *BeppoSAX* data show a preference of the broken power law model over the single power law; the latter was often the best fit in the *BeppoSAX* catalog, suggesting a long term change in the sources. The changes in the spectra of 3C 273 appear to be genuinely due to a variation in the state of the source, as well as in the case of AO 0235 – 164, observed during an outburst.

Four sources show intervening systems along the line of sight, but only one case is known to be gravitationally lensed. In the remaining three cases, it is not clear if the intervening galaxies can generate gravitational effects strong enough to enhance the γ−ray loudness. See Torres et al. (2003) for a discussion on this topic.

The SED compiled in the present sample confirm the model parameters already found in previous studies and increase the number of modelled sources. However, PKS 1406 – 076 shows some particular features and deserves further investigation. Four sources appear to be the key to understand the transition (with respect to γ−ray loudness) from blazars to radiogalaxies, namely 3C 273, PKS 0521 – 365, NGC 6251, and Cen A. The first two are FSRQ with the largest jet viewing angle, which in turn means the lowest δ among the blazars. The latter two are the (only) radiogalaxies detected by EGRET. Further and more detailed studies on these four sources could give important contributions to the comprehension of the mechanisms acting to generate γ−rays, of the unification models of AGN, and to the improvement of the resolution of the extragalactic γ−ray background.

Acknowledgements. LF thanks G.G.C. Palumbo, P. Grandi and M. Dadina for useful discussions and S.R. Rosen of the OM Team for useful hints in the OM data analysis. We thank also the referee, X. Barcons, for useful comments, that helped to improve the manuscript. This research has made use of the NASA's Astrophysics Data System Abstract Service and of the NASA/IPAC Extragalactic Database (NED), which is operated by the Jet Propulsion Laboratory, California Institute of Technology, under contract with the National Aeronautics and Space

Administration. This work was partly supported by the European Community's Human Potential Programme under contract HPRN-CT-2002-00321 and by the Italian Space Agency (ASI).

References

Aharonian F., Akhperjanian A.G., Aye K.M., et al., 2005a, A&A 436, L17
Aharonian F., Akhperjanian A.G., Bazer-Bachi A.R., et al., 2005b, submitted to Nature, (astro-ph/0508073)
Bechtold J., Siemiginowska A., Aldcroft T.L., et al., 2001, ApJ 562, 133
Bergeron J. & Boissé P., 1991, A&A 243, 344
Birkinshaw M., Worrall D.M. & Hardcastle M.J., 2002, MNRAS 335, 142
Böttcher M. & Dermer C.D., 2002, ApJ 564, 86
Böttcher M., Harvey J., Joshi M., et al., 2005, ApJ 631, 169
Brinkmann W., Sembay S., Griffits R.G., et al., 2001, A&A 365, L162
Brinkmann W., Papadakis I.E., den Herder J.W.A. & Haberl F., 2003, A&A 402, 929
Cagnoni I., Nicastro F., Maraschi L., Treves A. & Tavecchio F., 2004, ApJ 603, 449
Cappi M., Matsuoka M., Comastri A., et al., 1997, ApJ 478, 492
Cavaliere A. & D'Elia V., 2002, ApJ 571, 226
Chiaberge M., Capetti A. & Celotti A., 2001, MNRAS 324, L33
Chiaberge M., Gilli R., Capetti A. & Macchetto F.D., 2003, ApJ 597, 166
Cohen R.D., Smith H.E., Junkkarinen V.T. & Burbidge E.M., 1987, ApJ 318, 577
Courbin F., Meylan G., Kneib J.P. & Lidman C., 2002, ApJ 575, 95
Courvoisier T.J.-L., Beckmann V., Bourban G., et al., 2003, A&A 411, L343
Croston J.H., Hardcastle M.J., Birkinshaw M. & Worrall D.M., 2003, MNRAS, 346, 1041
Danziger I.J., Fosbury R.A.E., Goss W.M. & Ekers R.D., 1979, MNRAS 188, 415
De Rosa A., Piro L., Tramacere A., et al., 2005, A&A 438, 121
Dickey J.M. & Lockman F.J., 1990, ARA&A 28, 215
Donato D., Sambruna R.M. & Gliozzi M., 2005, A&A 433, 1163
Edelson R., Griffiths G., Markowitz A., et al., 2001, ApJ 554, 274
Evans D.A., Kraft R.P., Worrall D.M., et al., 2004, ApJ 612 786
Evans D.A., Worrall D.M., Hardcastle M.J., Kraft R.P. & Birkinshaw M., 2005, ApJ, accepted for publication (astro-ph/0512600)
Fabian A.C., Celotti A., Iwasawa K., et al., 2001, MNRAS 323, 373
Fang T., Marshall H.L., Bryan G.L. & Canizares C.R., 2001, ApJ 555, 356
Foschini L., Chiaberge M., Grandi P., et al., 2005, A&A, 433, 515
Foschini L., Ghisellini G., Raiteri C.M., et al., 2006, Proceedings of "The X-ray Universe", ed. A. Wilson, ESA SP-604, p. 615 (astro-ph/0510793)
Fossati G., Maraschi L., Celotti A., Comastri A. & Ghisellini G., 1998, MNRAS 299, 433
Ghisellini G., 2004, Nuclear Physics B Proceedings Supplements 132, 76
Ghisellini G., Celotti A., Fossati G., Maraschi L. & Comastri A., 1998, MNRAS 301, 451
Ghisellini G., Celotti A. & Costamante L., 2002, A&A 386, 833
Ghisellini G., Tavecchio F. & Chiaberge M., 2005, A&A 432, 401
Giommi P., Capalbi M., Fiocchi M., et al., 2002, Proceedings of Blazar Astrophysics with BeppoSAX and Other Observatories, eds P. Giommi, E. Massaro, G.G.C. Palumbo, ASI Science Data Center and ESA-ESRIN, p. 63 (astro-ph/0209596)
Giommi P., Colafrancesco S., Cavazzuti E., Perri M., Pittori C., 2006, A&A 445, 843
Gliozzi M., Sambruna R.M., Brandt W.N., et al., 2004, A&A 413, 139
Grandi P., Fiocchi M., Perola C.G., et al., 2003, ApJ 593, 160
Grandi P. & Palumbo G.G.C., 2004, Science 306, 998
Grandi P., Malaguti G. & Fiocchi M., 2005, ApJ, accepted for publication (astro-ph/0511784)
Guainazzi M., Grandi P., Comastri A. & Matt G., 2003, A&A 410, 131
Hardcastle M.J., Worrall D.M. & Birkinshaw M., 1999, MNRAS 305, 246
Hartman R.C., Bertsch D.L., Bloom S.D., et al., 1999, ApJS 123, 79
Hutchison J.M., Cawthorne T.V. & Gabuzda D.C., 2001, MNRAS 321, 525
Jansen F., Lumb D., Altieri B., et al., 2001, A&A 365, L1
Junkkarinen V.T., Cohen R.D., Beaver E.A., et al., 2004, ApJ 614, 658
Kirsch M., 2005. EPIC status of calibration and data analysis. XMM-SOC-CAL-TN-0018, v. 2.4, 11 February 2005.
Kuiper L., Hermsen W., Verbunt F., et al., 2000, A&A 359, 615
Lamb R.C. & Macomb D.J., 1997, ApJ 488, 872
Lane W., Smette A., Briggs F., et al., 1998, AJ 116, 26
Landt H., Perlman E.S. & Padovani P., 2006, ApJ, 637, 183
Lidman C., Courbin F., Meylan G., et al., 1999, ApJ 514, L57
Madejski G., Takahashi T., Tashiro M., et al., 1996, ApJ 459, 156
Malizia A., Bassani L., Dean A.J., et al., 2000, ApJ 531, 642
Maraschi L., Ciapi A., Fossati G., Tagliaferri G. & Treves A., 1995a, ApJ 443, 29
Maraschi L., Fossati G., Tagliaferri G. & Treves A., 1995b, ApJ 443, 578

Maraschi L., Tavecchio F., Cagnoni I., et al., 2002, In: New Visions of the X-ray Universe in the XMM-Newton and Chandra era. ESA-ESTEC, 2001 (astro-ph/0202418)
Maraschi L. & Tavecchio F., 2003, ApJ 593, 667
Mason K.O., Breeveld A., Much R., et al., 2001, A&A 365, L36
Mathur S. & Nair S., 1997, ApJ 484, 140
Molendi S. & Sembay S., 2003, Assessing the EPIC spectral calibration in the hard band with 3C 273 observation. XMM-SOC-CAL-TN-0036, March 2003.
Mukherjee R., Halpern J., Mirabal N. & Gotthelf E.V., 2002, ApJ 574, 693
Oshima T., Mitsuda K., Ota N., et al., 2001, ApJ 551, 929
Padovani P., Perlman E.S., Landr H., Giommi P. & Perri M., 2003, ApJ 588, 128
Page K.L., Turner M.J.L., Done C., et al., 2004, MNRAS 349, 57
Pei Y.C., Fall S.M. & Bechtold J., 1991, ApJ 378, 6
Pettini M., Smith L.J., Hunstead R.W. & King D.L., 1994, ApJ 426, 79
Perlman E., Madejski G., Georganopoulos M., et al., 2005, ApJ 625, 727
Pian E., Falomo R., Ghisellini G., et al., 1996, ApJ 459, 169
Pian E., Vacanti G., Tagliaferri G., et al., 1998, ApJ 492, L17
Pian E., Foschini L., Beckmann V., et al., 2005, A&A 429, 427
Piconcelli E. & Guainazzi M., 2005, A&A 442, L53
Protassov R., van Dyk D.A., Connors A., et al., 2002, ApJ 571, 545
Raiteri C.M., Villata M., Aller H.D., et al., 2001, A&A 377, 396
Raiteri C.M., Villata M., Tosti G., et al., 2003, A&A 402, 151
Raiteri C.M., Villata M., Ibrahimov M.A., et al., 2005, A&A 438, 39
Raiteri C.M., Villata M., Kadler M., et al., 2006, A&A, accepted for publication (astro-ph/0603364)
Ravasio M., Tagliaferri G., Ghisellini G. & Tavecchio F., 2004, A&A 424, 841
Reynolds C.S. & Nowak M.A., 2003, Physics Reports 377, 389
Sambruna R.M., Maraschi L. & Urry C.M., 1996, ApJ 463, 424
Sambruna R.M., Gliozzi M., Donato D., et al., 2004, A&A 414, 885
Sbarufatti B., Treves A., Falomo R., 2005, ApJ 635, 173
Sembay S., Edelson R., Markowitz A., et al., 2002, ApJ 574, 634
Siebert J., Brinkmann W., Drinkwater M.J., et al., 1998, MNRAS 301, 261
Siemiginowska A., Bechtold J., Aldcroft T.L., et al. 2002, ApJ 570, 543
Snowden S., Still M., Harrus I. et al., 2004. An introduction to XMM-Newton data analysis. Version 2.01, 23 July 2004.
Sowards-Emmerd D., Romani R.W. & Michelson P., 2003, ApJ 590, 109
Sowards-Emmerd D., Romani R.W., Michelson P. & Ulvestad J.S., 2004, ApJ 609, 564
Sowards-Emmerd D., Romani R.W., Michelson P., et al., 2005, ApJ 626, 95
Stanghellini C., O'Dea C.P., Dallacasa D., et al., 1998, A&ASS 131, 303
Stanghellini C., 2003, PASA 20, 118
Stickel M. & Kühr H., 1993, A&AS 100, 395
Strong A.W., Moskalenko I.V., Reimer O., 2004, ApJ 613, 956
Strüder L., Briel U., Dennerl K., et al., 2001, A&A 365, L18
Swanenburg B.N., Hermsen W., Bennett K., et al., 1978, Nature 275, 298
Tagliaferri G., Ghisellini G., Giommi P., et al., 2000, A&A 354, 431
Tagliaferri G., Ghisellini G. & Ravasio M., 2002, Proceedings of Blazar Astrophysics with BeppoSAX and Other Observatories, eds P. Giommi, E. Massaro, G.G.C. Palumbo, ASI Science Data Center and ESA-ESRIN, p. 11 (astro-ph/0207017)
Tagliaferri G., Ravasio M., Ghisellini G., et al., 2003, A&A 400, 477
Tavecchio F., Maraschi L., Ghisellini G., et al., 2000, ApJ 543, 535
Tavecchio F., Maraschi L., Ghisellini G., et al., 2002, ApJ 575, 137
Teräsranta H., Wiren S., Koivisto P., Saarinen V., & Hovatta T., 2005, A&A 440, 409
Thompson D.J., Bertsch D.L., Dingus B.L., et al., 1995, ApJS 101, 259
Tingay S.J. & Edwards P.G., 2002, AJ 124, 652
Torres D.F., Romero G.E., Eiroa E.F., Wambsganss J. & Pessah M.E., 2003, MNRAS 339, 335
Turner M.J., Abbey A., Arnaud M., et al., 2001, A&A 365, L27
Ulrich M.-H., Maraschi L., & Urry C.M., 1997, ARA&A 35, 445
Urry C.M. & Padovani P., 1995, PASP 107, 803
von Montigny C., Bertsch D.L., Chiang J., et al., 1995, ApJ 440, 525
Wagner S.J., & Witzel A., 1995, ARA&A 33, 163
Wiklind T. & Combes F., 1996, Nature 379, 11
Wolfe A.M., Gawiser E. & Prochaska J.X., 2005, ARA&A 43, 861
Wolter A., Tavecchio F., Caccianiga A., Ghisellini G. & Tagliaferri G., 2000, A&A 357, 429
Zhang Y.H., Treves A., Celotti A., Qin Y.P. & Bai J.M., 2005, ApJ 629, 686

Online Material

Appendix A: Notes on individual sources, tables and SED

We report in this Appendix the tables with the Observation log (Table A.1), the fit with the simple power law model (Table A.2), the broken power law model (Table A.3), the additional fits for 3C 273 (Table A.4 and A.5) and Cen A (Table A.6) and the magnitudes with different filters of the Optical Monitor (Table A.7). Some notes on the individual sources and the SED of the sources not reported in Sect. 6 (Fig. A.1 and A.2) complete this Appendix.

3EG J0222+4253 (0219+428, 3C 66A): The counterpart of this EGRET source is the BL Lac 0219 + 428, although Kuiper et al. (2000) have proposed that the flux below 300 MeV is significantly contaminated by the nearby pulsar PSR J0218+4232. 3C 66A was extensively monitored from radio to very high γ−rays during 2003−2004 (Böttcher et al. 2005) and no significant X-ray variability was detected. The present *XMM-Newton* data set was affected by a high background, but it is possible to use more than 70% of the observation. The fit of the spectrum of this BL Lac object with an absorbed power law model is acceptable (see Table A.2), although there are residuals for energies greater than 4 keV. The broken power law model provides the best fit with a confidence > 99.99% with a f-test. This observation has been studied by Croston et al. (2003) and the fit with a simple power law absorbed by the Galactic $N_{\rm H}$ is consistent with the present results. However, significant differences are present in the fit with the broken power law model: this can be understood by taking into account that in the present analysis a more conservative selection of events has been used (for example, this can be clearly inferred by comparing the PN exposures: 11 ks in the present analysis vs 15 ks in the analysis of Croston et al., 2003).

3EG J0237+1635 (AO 0235+164): The data set analyzed here refers to an observation performed in 2002 and shows no signs of high background. The `epatplot` task of `XMM SAS` shows a slight excess of double pixels events and a corresponding deficit of single pixel events (pile-up), that can be easily suppressed by removing the inner region with 5″ radius. The fit can improve significantly by reducing the energy band to 1 – 10 keV, that is by removing the energy band that can be affected by the absorption and the fit reported in Tables A.2 and A.3 refer to this case. The best fit is still obtained with the broken power law model with the absorption column fixed to the Galactic value, although the Γ_1 is slightly harder than the above mentioned case.

3EG J0530-3626 (PKS 0521-365): The blazar PKS 0521 – 365 has been associated with the EGRET source in the Second Catalog (Thompson et al. 1995), but a stronger detection in the Cycle 4 placed this blazar outside the 99.99% probability contours. Sowards-Emmerd et al. (2004) suggested that the counterpart of 3EG J0530 – 3626 source could be another radio source (PMN J0529−3555) of unknown nature. This can be another case of a possible double source not resolved by EGRET (like, e.g. 3EG J0222 + 4253), an interesting target worth observing with *GLAST*. In the present work, we keep as valid the association with PKS 0521 − 365. The *XMM-Newton* observation is analyzed here for the first time. There is no evidence of high background, but the `epatplot` task shows that the data are affected by pile-up. This blazar has a small jet (6″), visible in radio (see Tingay & Edwards 2002 for a description of the parsec scale structure), and optical wavelenghts (Danziger et al. 1979). *Chandra* detected a jet-like feature of 2″-size, spatially coincident with the optical and radio structure (Birkinshaw et al. 2002). Hardcastle et al. (1999) and Birkinshaw et al. (2002) reported also the presence of extended emission that can be fitted with thermal plasma model with $kT = 1.6$ keV and $Z_\odot = 0.05$. Given the size of the PSF of EPIC camera on board *XMM-Newton* (12″ – 15″ HEW, see Jansen et al. 2001), the above mentioned structures are not resolved. Attempts to fit the low energy part with a thermal plasma model (`mekal` or `raymond` models in `xspec`, not reported in the Tables), resulted in a $\tilde{\chi}^2 \approx 1.08$ improved with respect to the simple power law ($\Delta\chi^2 = 84$ for a decrease of 2 dof), but still worse than the broken power law model. The broken power law model absorbed by the Galactic column provides the best fit to the present data, consistent with the results obtained by *Einstein*, *EXOSAT* (Pian et al. 1996), *ROSAT* (Pian et al. 1996, Hardcastle et al. 1999), *BeppoSAX* (Tavecchio et al. 2002).

3EG J0721+7120 (S5 0716+714): This BL Lac object is known for its extreme variability, also at intraday time scales (cf Wagner & Witzel 1995), and it is extensively monitored by optical and radio ground telescopes (see, e.g. Raiteri et al. 2003). The present observation was performed simultaneously with the end of a ToO of *INTEGRAL*, triggered after an optical giant flare (Pian et al. 2005). The optical lightcurve started to increase at the end of March 2004, and the trigger was activated on 27 March. The *INTEGRAL* ToO was performed from 2 to 7 April, when the source activity was already declining. The *XMM-Newton* observation covered instead the period 4 – 5 April. The X-ray lightcurve shows a clear decrease of the flux as the observation proceeded, confirming that the source was observed during the tail of the flare. More details on this *XMM-Newton* data set are presented in a separate paper (Foschini et al., submitted).

3EG J0845+7049 (S5 0836+710): This flat-spectrum radio quasar has one of the highest redshifts among the objects in the present sample. The *XMM-Newton* data, published here for the first time, show high background. Past analyses of *ROSAT* and *ASCA* data by Cappi et al. (1997) and *BeppoSAX* data by Tavecchio et al. (2000) have shown a spectrum with a hard photon index ($\Gamma \approx 1.3$), with acceptable fit also with a broken power law, but some inconsistencies in the value of the absorption. The present data are best fitted with a simple power law model absorbed by the Galactic column plus an additional absorber at the redshift of the quasar with a value $(1.4\pm0.3)\times10^{21}$ cm^{-2}, consistent with the *ASCA* and *BeppoSAX* values. This is also consistent with *Chandra* observations by Fang et al. (2001), who found $\Gamma = 1.388 \pm 0.012$ (0.5 – 8 keV), but a slightly lower absorption $N_{\rm H} = (7.0 \pm 1.2) \times 10^{20}$ cm^{-2} (not redshifted). The photon index is also consistent with the

Table A.1. *XMM-Newton* Observation Log. Columns: (1) Source name; (2) Observation Identifier; (3) Date of the observation [DD-MM-YYYY]; (4,5,6) Observing mode of MOS1, MOS2, and PN, respectively [FF: Full Frame; SW: Small Window; TIMING: timing mode, without imaging] with the effective exposure time [ks]; (7) Angular distance from the boresight [arcsec].

Name	ObsID	Date	MOS1	MOS2	PN	Position
(1)	(2)	(3)	(4)	(5)	(6)	(7)
0219 + 428	0002970201	05 – 02 – 2002	FF(10)	FF(10)	FF(11.0)	366
AO 0235 + 164	0110990101	10 – 02 – 2002	FF(19)	FF(19)	FF(15.0)	77
PKS 0521 – 365	0065760201	09 – 10 – 2002	SW(31.3)	FF(31.3)	FF(27.1)	65
S5 0716 + 714	0150495601	04 – 04 – 2004	SW(31)	FF(31)	TIMING	69
S5 0836 + 710	0112620101	12 – 04 – 2001	SW(23.8)	SW(23.8)	FF(24.6)	14
Mkn 421[a]	0099280201	01 – 11 – 2000	SW	SW	SW(24.2)	6.5
	0099280301	13 – 11 – 2000	SW	SW	SW(25.6)	7.1
	0099280401	14 – 11 – 2000	SW	SW	SW(23.4)	119.7
	0136540101	08 – 05 – 2001	SW	SW	SW(25.7)	4.7
	0158970101	01 – 06 – 2003	TIMING	SW	SW(25.3)	6.1
	0162960101	10 – 12 – 2003	SW	SW	SW(17.4)	6.4
PKS 1127 – 145	0112850201	01 – 07 – 2002	FF(13.9)	FF(13.7)	FF(10.7)	68
ON 231	0104860501	26 – 06 – 2002	FF(33.1)	FF(32.6)	FF(26.7)	472
3C 273[a]	0126700301	13 – 06 – 2000	SW	SW	SW(39.7)	10
	0126700601	15 – 06 – 2000	SW	SW	SW(20.8)	9
	0126700701	15 – 06 – 2000	SW	SW	SW(21.0)	8
	0126700801	17 – 06 – 2000	SW	SW	SW(42.5)	9
	0136550101	13 – 06 – 2001	SW	SW	SW(62.0)	5
	0112770101	16 – 12 – 2001	TIMING	SW	SW(3.5)	54.8
	0112770201	22 – 12 – 2001	TIMING	SW	SW(3.5)	54.5
	0112770601	07 – 07 – 2002	TIMING	SW	SW(3.5)	78.7
	0112770801	17 – 12 – 2002	TIMING	SW	SW(3.5)	55.0
	0136550501	05 – 01 – 2003	SW	SW	SW(6.0)	5
	0112770701	05 – 01 – 2003	TIMING	SW	SW(3.5)	58.8
	0112771001	18 – 06 – 2003	TIMING	SW	SW(3.9)	79.1
	0112770501	08 – 07 – 2003	TIMING	SW	SW(5.6)	78.0
	0112771101	14 – 12 – 2003	TIMING	SW	SW(5.9)	57.2
	0136550801	30 – 06 – 2004	SW	SW	SW(13.9)	3
Cen A	0093650201	02 – 02 – 2001	FF(22.8)	FF(22.8)	FF(16.8)	9
	0093650301	06 – 02 – 2002	FF(13.2)	FF[b]	FF(7.9)	16
PKS 1334 – 127	0147670201	31 – 01 – 2003	FF(13.5)	FF(13.5)	FF(10.9)	68
PKS 1406 – 076	0151590101	05 – 07 – 2003	FF(7.8)	FF(10.0)	FF(7.3)	68
	0151590201	10 – 08 – 2003	FF(5.6)	FF(5.8)	FF(3.6)	69
NGC 6251	0056340201	26 – 03 – 2002	FF(18.0)	FF(18.0)	FF(8.0)	69
PKS 1830 – 211	0204580201	10 – 03 – 2004	FF(7.0)	FF(7.6)	FF(2.8)	67
	0204580301	24 – 03 – 2004	FF(31.0)	FF(31.0)	FF(27.0)	68
	0204580401	05 – 04 – 2004	FF(18.5)	FF(18.5)	FF(13.0)	68
PKS 2155 – 304[a]	0124930201	31 – 05 – 2000	TIMING	SW	SW(41.6)	9
	0080940101	19 – 11 – 2000	TIMING	SW	SW(40.2)	10
	0080940301	20 – 11 – 2000	TIMING	SW	SW(40.8)	16
	0124930301	30 – 11 – 2001	SW	SW	SW(31.2)	15
	0124930501	24 – 05 – 2002	SW	SW	SW(22.3)	6
	0124930601	29 – 11 – 2002	SW	SW	SW(39.8)	2
	0158960101	23 – 11 – 2003	SW	SW	SW(18.7)	5
	0158960901	22 – 11 – 2004	SW	SW	SW(20.0)	6
	0158961001	23 – 11 – 2004	SW	SW	SW(28.0)	6

[a] Only PN data have been analyzed, because the high flux of the source caused strong pile-up.
[b] MOS2 not used, because of a series of bad pixels in the source PSF.

value of $\Gamma = 1.3 \pm 0.3$ in the $20 - 100$ keV energy band measured by *INTEGRAL* (Pian et al. 2005) and the value of $\Gamma = 1.1 \pm 0.3$ measured by *CGRO* with OSSE and BATSE instruments (Malizia et al. 2000). The broken power law gives also a good fit, although with no improvement with respect to the simple power law model, but does not require the additional absorber.

3EG J1104+3809 (Mkn 421): This is one of three sources in the present sample that has been extensively observed, being

Table A.2. Fit results with single powerl law model. Columns: (1) Source name; (2) absorbing column density [10^{20} cm^{-2}]; (3) photon index of the power law; (4) Normalization of the power law model [10^{-2} ph cm^{-2} s^{-1} keV^{-1} at 1 keV]; (5) Reduced χ^2 and degrees of freedom; (6) observed flux in the 0.4 – 10 keV energy band [10^{-11} erg cm^{-2} s^{-1}]; (7) intrinsic luminosity in the 0.4 – 10 keV energy band rest frame [10^{45} erg s^{-1}]. The uncertainties in the parameter estimates are at the 90% confidence limits for 1 parameter. For $N_{\rm H}$ = Gal, it means that the absorption column has been fixed to the Galactic value.

Name	$N_{\rm H}$	Γ	A	$\tilde{\chi}^2$/dof	F	L
(1)	(2)	(3)	(4)	(5)	(6)	(7)
0219 + 428	Gal.	2.60 ± 0.04	0.183 ± 0.007	1.29/293	0.21	2.6
AO 0235 + 164	Gal.	2.28 ± 0.02	1.22 ± 0.04	0.99/618	0.96	66
PKS 0521 – 365	Gal.	1.847 ± 0.009	0.231 ± 0.002	1.15/1202	1.2	9.0×10^{-4}
S5 0716 + 714[a]	Gal.	2.58 ± 0.02	0.294 ± 0.003	1.74/419	1.0	> 14.2
S5 0836 + 710[b]	14 ± 3	1.379 ± 0.007	2.62 ± 0.04	1.07/2272	4.8	902
Mkn 421[c]	2.3 ± 0.3	2.61 ± 0.01	7.74 ± 0.09	0.97/1026	26.0	0.59
	3.5 ± 0.2	2.438 ± 0.006	26.3 ± 0.1	1.20/1491	90.6	2.12
	3.1 ± 0.2	2.457 ± 0.006	25.6 ± 0.1	1.29/1430	88.8	2.05
	3.1 ± 0.2	2.373 ± 0.007	18.3 ± 0.1	1.12/1447	66.1	1.51
	4.6 ± 0.2	2.73 ± 0.01	13.5 ± 0.1	1.16/1178	40.6	1.02
	3.7 ± 0.2	2.43 ± 0.01	16.3 ± 0.1	1.03/1307	56.0	1.31
PKS 1127 – 145[d]	12^{+2}_{-1}	1.31 ± 0.02	0.34 ± 0.01	1.01/890	1.1	59.2
ON 231	2.5 ± 0.6	2.77 ± 0.04	0.186 ± 0.005	1.07/653	0.50	0.16
3C 273	Gal.	1.829 ± 0.004	2.788 ± 0.007	1.82/1598	12.2	8.4
	Gal.	1.819 ± 0.005	2.68 ± 0.01	1.71/1401	11.8	8.2
	Gal.	1.812 ± 0.005	2.603 ± 0.009	1.53/1394	11.5	8.0
	Gal.	1.8 ± 0.2	2.599 ± 0.004	2.08/1647	11.5	8.0
	Gal.	1.9 ± 0.2	3.634 ± 0.004	4.22/1711	14.5	10.2
	Gal.	1.87 ± 0.01	4.18 ± 0.03	1.24/802	17.4	12.2
	Gal.	1.82 ± 0.01	3.97 ± 0.03	1.15/806	17.5	12.1
	Gal.	1.89 ± 0.01	3.09 ± 0.02	1.08/680	12.7	8.90
	Gal.	1.98 ± 0.01	4.67 ± 0.03	1.21/790	17.7	12.6
	Gal.	2.019 ± 0.009	3.92 ± 0.02	1.37/899	14.3	10.3
	Gal.	2.02 ± 0.01	3.99 ± 0.03	1.23/711	14.5	10.4
	Gal.	1.950 ± 0.009	4.78 ± 0.03	1.27/826	18.5	13.2
	Gal.	1.963 ± 0.008	4.13 ± 0.02	1.12/908	15.8	11.2
	Gal.	1.901 ± 0.009	3.07 ± 0.02	1.33/877	12.5	8.77
	Gal.	1.899 ± 0.006	2.64 ± 0.01	1.32/1160	10.7	7.54
Cen A[e]	1400 ± 200	2.2 ± 0.1	22^{+7}_{-5}	0.97/668	16.9	3.0×10^{-4}
	1800 ± 300	2.3 ± 0.2	29^{+14}_{-9}	0.97/340	18.5	3.3×10^{-4}
PKS 1334 – 127	6.7 ± 0.9	1.80 ± 0.04	0.171 ± 0.009	0.93/609	0.43	5.1
PKS 1406 – 076	Gal.	1.58 ± 0.07	$0.060^{+0.007}_{-0.006}$	0.79/90	0.10	10.5
	Gal.	1.6 ± 0.1	$0.056^{0.009}_{-0.007}$	0.94/49	0.094	9.78
NGC 6251	$11.6^{+0.8}_{-0.7}$	1.94 ± 0.03	0.134 ± 0.004	1.04/812	0.577	9.6×10^{-3}
PKS 1830 – 211[d]	350 ± 50	$1.17^{+0.03}_{-0.05}$	$0.62^{+0.07}_{-0.08}$	0.90/600	1.42	322
	240 ± 10	1.14 ± 0.02	0.54 ± 0.03	1.04/1662	1.34	290
	220 ± 10	1.13 ± 0.03	0.47 ± 0.03	1.04/1168	1.22	261
PKS 2155 – 304[c]	1.6 ± 0.2	2.592 ± 0.009	5.12 ± 0.04	1.02/1266	14.4	5.71
	2.2 ± 0.2	2.81 ± 0.01	4.49 ± 0.04	1.00/1067	11.6	4.87
	1.9 ± 0.3	2.86 ± 0.01	3.61 ± 0.04	1.03/991	9.32	3.90
	3.2 ± 0.2	2.868 ± 0.009	8.23 ± 0.06	1.01/1131	20.2	8.89
	1.4 ± 0.3	2.70 ± 0.01	3.68 ± 0.05	0.99/886	10.0	4.02
	3.0 ± 0.3	2.89 ± 0.01	2.81 ± 0.04	0.87/880	6.90	3.03
	Gal.	2.96 ± 0.01	2.40 ± 0.01	0.95/614	6.17	2.60
	2.5 ± 0.5	3.08 ± 0.02	2.80 ± 0.05	0.88/625	6.83	3.04
	2.9 ± 0.4	2.98 ± 0.02	3.77 ± 0.05	1.10/831	9.14	4.07

[a] Only MOS1+MOS2, since the PN was set in TIMING. Lower limit of luminosity calculated for $z = 0.5$.
[b] Additional absorber placed at the redshift of the source (`wa*zwa(zpo)` model in `xspec`).
[c] Fit in the 0.6 – 10 keV energy range and extrapolation to 0.4 keV for flux and luminosity calculations.
[d] Additional redshifted absorber (`wa*zwa(zpo)` model in `xspec`) along the line of sight.
[e] Fit in the 4 – 10 keV energy range, without 6 – 8 keV energy band, because of complex features in the low energy part and in the iron emission line complex.

Table A.3. Fit results with the broken power law model. Columns: (1) Source name; (2) absorbing column density [10^{20} cm^{-2}]; (3) low energy photon index of the power law; (4) high energy photon index; (5) Break energy [keV]; (6) Normalization of the power law model [10^{-2} ph cm^{-2} s^{-1} keV^{-1} at 1 keV]; (7) Reduced χ^2 and degrees of freedom; (8) observed flux in the 0.4 – 10 keV energy band [10^{-11} erg cm^{-2} s^{-1}]; (9) intrinsic luminosity in the 0.4 – 10 keV energy band rest frame [10^{45} erg s^{-1}]; (10) Ftest probability [%]; fit with probability below 90% are not reported. The uncertainties in the parameter estimates are at the 90% confidence limits for 1 parameter. For $N_{\rm H}$ = Gal, it means that the absorption column has been fixed to the Galactic value.

Name	$N_{\rm H}$	Γ_1	Γ_2	$E_{\rm break}$	A	$\tilde{\chi}^2$/dof	F	L	*Ftest*
(1)	(2)	(3)	(4)	(5)	(6)	(7)	(8)	(9)	(10)
0219 + 428	Gal.	$2.91^{+0.12}_{-0.08}$	$2.23^{+0.10}_{-0.09}$	1.3 ± 0.2	0.067 ± 0.003	1.05/291	0.24	3.0	> 99.99
AO 0235 + 164	Gal.	2.33 ± 0.04	2.1 ± 0.1	$3.3^{+0.7}_{-0.5}$	0.276 ± 0.006	0.96/616	0.99	69	> 99.99
PKS 0521 – 365	Gal.	1.95 ± 0.03	1.74 ± 0.03	$1.5^{+0.3}_{-0.2}$	0.227 ± 0.003	1.05/1200	1.3	9.4×10^{-4}	99.97
S5 0716 + 714[a]	Gal.	2.70 ± 0.02	$1.98^{+0.08}_{-0.09}$	$2.3^{+0.2}_{-0.1}$	0.293 ± 0.003	1.06/417	1.1	> 15.7	> 99.99
S5 0836 + 710	Gal.	1.25 ± 0.03	1.375 ± 0.007	$1.01^{+0.15}_{-0.08}$	0.529 ± 0.006	1.07/2271	4.8	860	-
Mkn 421[b]	Gal.	2.573 ± 0.008	$2.79^{+0.17}_{-0.08}$	$4.2^{+1.0}_{-0.7}$	6.97 ± 0.02	0.96/1025	26.1	0.578	99.97
	Gal.	2.340 ± 0.004	2.73 ± 0.04	4.0 ± 0.2	22.9 ± 0.4	1.06/1490	91.3	2.00	> 99.99
	Gal.	$2.378^{+0.004}_{-0.005}$	$2.96^{+0.08}_{-0.10}$	$4.7^{+0.2}_{-0.3}$	22.6 ± 0.4	1.02/1429	89.1	1.95	> 99.99
	Gal.	2.312 ± 0.007	$2.68^{+0.07}_{-0.05}$	4.4 ± 0.3	16.4 ± 0.7	0.99/1446	66.7	1.45	> 99.99
	Gal.	$2.59^{+0.01}_{-0.02}$	2.81 ± 0.02	$2.2^{+0.1}_{-0.2}$	$11.5^{+0.7}_{-0.8}$	1.08/1177	41.8	0.929	> 99.99
	Gal.	2.300 ± 0.007	2.51 ± 0.02	2.2 ± 0.1	14.1 ± 0.4	0.99/1306	56.3	1.23	> 99.99
PKS 1127 – 145[c]	12^{+2}_{-1}	$1.40^{+0.08}_{-0.05}$	1.22 ± 0.06	$2.7^{+1.0}_{-0.8}$	$0.127^{+0.006}_{-0.004}$	1.00/888	1.2	61.0	99.58
ON 231	Gal.	2.74 ± 0.02	$2.3^{+0.3}_{-0.4}$	$4.2^{+0.9}_{-1.1}$	0.140 ± 0.002	1.07/652	0.51	0.16	94.50
3C 273	Gal.	1.943 ± 0.009	1.697 ± 0.009	1.48 ± 0.06	2.073 ± 0.008	1.13/1596	12.7	8.7	> 99.99
	Gal.	1.97 ± 0.01	1.65 ± 0.01	1.43 ± 0.08	1.97 ± 0.01	1.03/1399	12.5	8.6	> 99.99
	Gal.	1.96 ± 0.01	1.67 ± 0.01	1.35 ± 0.08	1.91 ± 0.01	1.00/1392	12.1	8.3	> 99.99
	Gal.	1.92 ± 0.01	1.654 ± 0.009	1.37 ± 0.05	1.911 ± 0.008	0.97/1645	12.2	8.4	> 99.99
	Gal.	2.121 ± 0.007	1.676 ± 0.008	1.45 ± 0.03	2.604 ± 0.009	1.10/1709	15.7	11.0	> 99.99
	Gal.	2.00 ± 0.02	1.72 ± 0.02	$1.4^{+0.2}_{-0.1}$	3.06 ± 0.03	1.00/800	18.4	12.7	> 99.99
	Gal.	1.94 ± 0.03	1.67 ± 0.03	1.5 ± 0.2	2.95 ± 0.03	0.95/804	18.4	12.6	> 99.99
	Gal.	1.97 ± 0.03	$1.79^{+0.03}_{-0.04}$	$1.4^{+0.4}_{-0.2}$	2.29 ± 0.03	1.01/678	13.1	9.09	> 99.99
	Gal.	2.09 ± 0.02	1.81 ± 0.03	1.6 ± 0.1	3.39 ± 0.03	0.97/788	18.6	13.2	> 99.99
	Gal.	2.16 ± 0.02	$1.83^{+0.02}_{-0.03}$	$1.4^{+0.2}_{-0.1}$	2.80 ± 0.03	0.99/897	15.1	10.8	> 99.99
	Gal.	2.13 ± 0.02	$1.81^{+0.04}_{-0.05}$	$1.7^{+0.3}_{-0.2}$	2.88 ± 0.03	0.96/709	15.4	10.9	> 99.99
	Gal.	2.05 ± 0.02	1.76 ± 0.03	1.8 ± 0.2	3.51 ± 0.03	1.02/824	19.5	13.7	> 99.99
	Gal.	2.02 ± 0.02	$1.82^{+0.03}_{-0.07}$	$1.9^{+0.6}_{-0.3}$	3.05 ± 0.02	1.00/906	16.4	11.6	> 99.99
	Gal.	2.02 ± 0.02	1.70 ± 0.03	$1.7^{+0.2}_{-0.1}$	2.26 ± 0.02	1.02/875	13.2	9.20	> 99.99
	Gal.	$2.00^{+0.02}_{-0.01}$	1.76 ± 0.02	$1.5^{+0.2}_{-0.1}$	1.94 ± 0.01	1.03/1158	11.2	7.8	> 99.99
Cen A									-
									-
PKS 1334 – 127	Gal.	$1.57^{+0.08}_{-0.24}$	1.78 ± 0.03	1.0 ± 0.3	$0.077^{+0.012}_{-0.003}$	0.92/608	0.43	4.8	92.31
PKS 1406 – 076									81.60
									56.30
NGC 6251	14 ± 1	$2.11^{+0.08}_{-0.06}$	1.78 ± 0.07	$2.5^{+0.3}_{-0.4}$	0.141 ± 0.004	1.00/810	0.59	0.010	> 99.99
PKS 1830 – 211	62^{+5}_{-6}	$0.93^{+0.08}_{-0.10}$	$1.42^{+0.10}_{-0.05}$	$3.6^{+0.4}_{-0.5}$	0.11 ± 0.01	0.83/598	1.38	270	> 99.99
	62 ± 3	$0.89^{+0.06}_{-0.09}$	1.29 ± 0.04	3.1 ± 0.3	$0.103^{+0.06}_{-0.08}$	0.97/1660	1.31	243	> 99.99
	64 ± 3	1.06 ± 0.04	$1.41^{+0.12}_{-0.09}$	$4.7^{+0.5}_{-0.4}$	0.108 ± 0.06	1.00/1166	1.20	248	> 99.99
PKS 2155 – 304[b]	Gal.	2.588 ± 0.005	$2.73^{+0.18}_{-0.08}$	$4.4^{+1.4}_{-1.1}$	3.861 ± 0.008	1.01/1265	14.3	5.70	> 99.99
	Gal.	$2.773^{+0.007}_{-0.006}$	$2.88^{+0.06}_{-0.03}$	$2.8^{+0.7}_{-0.4}$	3.246 ± 0.007	0.98/1066	11.6	4.74	> 99.99
	Gal.	2.845 ± 0.006	3.0 ± 0.1	$4.3^{+0.8}_{-1.2}$	2.620 ± 0.007	1.02/990	9.31	3.86	99.67
	Gal.	2.783 ± 0.006	2.96 ± 0.04	$2.4^{+0.3}_{-0.2}$	5.75 ± 0.01	0.97/1130	20.3	8.35	> 99.99
	Gal.	2.75 ± 0.03	$2.70^{+0.01}_{-0.02}$	$1.0^{+0.5}_{-0.1}$	2.74 ± 0.02	0.99/885	10.0	4.10	96.01
									-
									89.10
									-
									85.00

[a] Only MOS1+MOS2, since the PN was set in TIMING. Lower limit of luminosity calculated for $z = 0.5$.
[b] Fit in the 0.6 – 10 keV energy range and extrapolation to 0.4 keV for flux and luminosity calculations.
[c] Additional redshifted absorber (`wa*zwa(bknpo)` model in `xspec`) along the line of sight.

Table A.4. Additional fit results for 3C 273 (3EG J1229 + 0210) with the model composed of a black body plus a power law (`wa(zbb+zpo)`), absorbed with the Galactic column density. Columns: (1) Temperature [keV]; (2) Normalization of the black body model [$10^{-4} L_{39}/D_{10}^2$, where L_{39} is the source luminosity in units of 10^{39} erg/s and D_{10} is the source distance in units of 10 kpc]; ; (3) Photon index; (4) Normalization of the power law model [10^{-2} ph cm^{-2} s^{-1} keV^{-1} at 1 keV]; (5) Reduced χ^2 and degrees of freedom; (6) observed flux in the 0.4 – 10 keV energy band [10^{-11} erg cm^{-2} s^{-1}]; (7) intrinsic luminosity in the 0.4 – 10 keV energy band rest frame [10^{45} erg s^{-1}]. The uncertainties in the parameter estimates are at the 90% confidence limits for 1 parameter.

kT	$A_{\rm zbb}$	Γ	$A_{\rm pl}$	$\tilde{\chi}^2$/dof	F	L
(1)	(2)	(3)	(4)	(5)	(6)	(7)
0.143 ± 0.004	1.48 ± 0.07	1.714 ± 0.005	2.47 ± 0.02	1.17/1596	12.6	8.7
0.143 ± 0.004	$1.82^{+0.09}_{-0.10}$	1.668 ± 0.007	2.29 ± 0.03	1.06/1399	12.5	8.6
$0.138^{+0.006}_{-0.004}$	$1.58^{+0.11}_{-0.08}$	$1.685^{+0.006}_{-0.008}$	$2.28^{+0.02}_{-0.04}$	1.01/1392	12.1	8.3
0.137 ± 0.004	$1.76^{+0.06}_{-0.10}$	1.669 ± 0.009	2.25 ± 0.02	1.02/1645	12.2	8.3
0.140 ± 0.002	3.47 ± 0.07	1.701 ± 0.005	2.93 ± 0.02	1.23/1709	15.7	10.9
$0.152^{+0.007}_{-0.008}$	2.8 ± 0.3	1.72 ± 0.02	3.54 ± 0.09	0.99/800	18.4	12.7
0.153 ± 0.009	2.3 ± 0.3	1.68 ± 0.02	3.42 ± 0.09	0.95/804	18.3	12.5
0.16 ± 0.01	1.4 ± 0.3	$1.79^{+0.01}_{-0.02}$	2.76 ± 0.08	1.00/678	13.1	9.06
$0.149^{+0.007}_{-0.008}$	$3.1^{+0.3}_{-0.4}$	1.82 ± 0.02	4.0 ± 0.1	0.98/788	18.6	13.1
0.136 ± 0.006	2.9 ± 0.2	1.86 ± 0.01	3.36 ± 0.07	1.02/897	15.0	10.7
0.148 ± 0.007	3.1 ± 0.3	1.84 ± 0.02	3.33 ± 0.09	0.95/709	15.3	10.9
$0.146^{+0.007}_{-0.008}$	3.0 ± 0.3	$1.80^{+0.01}_{-0.02}$	4.13 ± 0.09	1.04/824	19.4	13.6
0.157 ± 0.008	2.0 ± 0.3	$1.852^{+0.009}_{-0.017}$	3.67 ± 0.08	0.99/906	16.3	11.5
0.146 ± 0.007	2.1 ± 0.2	1.74 ± 0.02	2.61 ± 0.06	1.04/875	13.1	9.13
0.151 ± 0.005	1.6 ± 0.1	1.762 ± 0.008	2.28 ± 0.04	1.00/1158	11.2	7.8

Table A.5. Detections and upper limits on the equivalent width of iron lines for 3C 273 (3EG J1229 + 0210). The continuum is best fitted with the broken power law model with Galactic absorbtion reported in Table A.3. Columns: (1) Equivalent width [eV] for $E = 6.4$ keV and $\sigma = 0.15$ keV; (2) $\Delta\chi^2$ with respect to the best fit continuum (2 dof); (3) Equivalent width [eV] for $E = 6.4$ keV and $\sigma = 0.5$ keV; (4) $\Delta\chi^2$ with respect to the best fit continuum (2 dof); (5) Equivalent width [eV] for $E = 6.7$ keV and $\sigma = 0.15$ keV; (6) $\Delta\chi^2$ with respect to the best fit continuum (2 dof); (7) Equivalent width [eV] for $E = 6.7$ keV and $\sigma = 0.5$ keV; (8) $\Delta\chi^2$ with respect to the best fit continuum (2 dof); The uncertainties in the parameters and upper limits estimate are at the 90% confidence limits for 1 parameter.

$E = 6.4$ keV				$E = 6.7$ keV			
$\sigma = 0.15$ keV	$\Delta\chi^2$	$\sigma = 0.5$ keV	$\Delta\chi^2$	$\sigma = 0.15$ keV	$\Delta\chi^2$	$\sigma = 0.5$ keV	$\Delta\chi^2$
(1)	(2)	(3)	(4)	(5)	(6)	(7)	(8)
29^{+13}_{-12}	14.3	54.5 ± 0.1	20.2	18.4 ± 0.1	5.2	39.3 ± 0.1	7.7
< 16	–	< 50	–	< 28	–	< 53	–
< 19	–	< 62	–	31 ± 19	7.2	< 64	–
20^{+13}_{-12}	7.0	46^{+33}_{-15}	16.0	21^{+13}_{-14}	6.4	62^{+15}_{-36}	12.5
< 20	–	38^{+27}_{-13}	16.2	22 ± 11	10.8	48^{+13}_{-28}	12.0
< 37	–	< 59	–	< 46	–	< 83	–
< 56	–	< 87	–	< 30	–	< 95	–
< 38	–	< 105	–	< 41	–	< 113	–
44^{+40}_{-37}	3.3	< 117	–	< 42	–	< 133	–
< 62	–	80^{+49}_{-67}	4.1	64^{+34}_{-37}	8.6	110^{+44}_{-83}	5.8
< 52	–	< 144	–	< 75	–	< 156	–
< 42	–	< 111	–	< 60	–	< 112	–
< 60	–	< 106	–	43^{+34}_{-35}	4.1	< 92	–
< 40	–	< 97	–	< 55	–	< 125	–
< 40	–	33^{+68}_{-26}	3.8	< 47	–	33^{+74}_{-27}	3.7

a calibration target (the others are 3C 273 and PKS 2155 – 304). 32 observations are present in the *XMM-Newton* data archive, but for sake of homogeneity in the present analysis, we selected only the 6 observations with EPIC PN in small window mode. We refer the reader to the several papers published with more detailed analysis of Mkn 421 data with different observing modes (e.g. Brinkmann et al. 2001, 2003, Sembay et al. 2002, Ravasio et al. 2004).

3EG J1134-1530 (PKS 1127-145): This source is in the list of Gigahertz-Peaked Sources (GPS) by Stanghellini et al. (1998), Stanghellini (2003). The present *XMM-Newton* data set has never been published. It shows high background, but, once

cleaned of soft-proton flares, it is possible to extract useful information. This source also has a 30″-sized jet, observed in X-rays with *Chandra* (Siemiginowska et al. 2002), but that is still too small for the PSF size of EPIC.

3EG J1222+2841 (ON 231): This is another EGRET source that could be composed of two or more contributions: indeed, although ON 231 is outside the global 99% probability contours of 3EG J1222 + 2841, there is a strong association with the emission at $E > 1$ GeV (Lamb & Macomb 1997). The present *XMM-Newton* data set has never been analysed and shows evidence of high background towards the end of the observation. The broken power law model provides the best fit to the data. An absorption in addition to the Galactic column is marginally detected. The values are consistent with, although slightly different to the fit to the *BeppoSAX* data of an observation in 1998, when ON 231 was in outburst (Tagliaferri et al. 2000).

3EG J1229+0210 (3C 273): For historical reasons, 3C 273 is one of the most observed sources in the sky, and *XMM-Newton* spent a lot of time observing this quasar (3C 273 is also a calibration source). We refer the reader to the works by Molendi & Sembay (2003), Courvoisier et al. (2003) and Page et al. (2004) for more details in the analysis of the *XMM-Newton* data sets. There is a general agreement between the analysis presented here and the above cited works: just to mention one case (ObsID 0136550501), for the fit with a simple power law model with the Galactic absorption column in the 3 – 10 keV energy band, Courvoisier et al. (2003) reported $\Gamma = 1.74 \pm 0.03$, Page et al. (2004) found $\Gamma = 1.78 \pm 0.02$, and the value in the present work is $\Gamma = 1.79 \pm 0.06$. However, small differences in the procedures should be noted. Indeed, a small excess of double pixel events and a corresponding deficit of single pixel events can be observed with `epatplot` task at high energies, specifically above 8 keV, as already indicated by Molendi & Sembay (2003). The problem is resolved by removing the inner region of 8″ radius: the fit improves with negligible changes in the spectral parameters. For example, let us consider the data of the ObsID 0112770101 in the 3 – 10 keV energy band fit with a simple power law model with Galactic absorption. By using a circular region with 40″ radius, the best fit gives these values: $\Gamma = 1.69 \pm 0.05$ and normalization 0.033 ± 0.003 ph cm^{-2} s^{-1} keV^{-1} for $\tilde{\chi}^2 = 1.08$ and 588 dof. This is to be compared with $\Gamma = 1.73 \pm 0.07$ and normalization 0.036 ± 0.004 ph cm^{-2} s^{-1} keV^{-1} for $\tilde{\chi}^2 = 0.97$ and 315 dof in the case of annular region of extraction with inner radius 8″ and external radius 40″. Therefore, since the fit improves significantly with a small increase of the error bars, the annular region of extraction has been used in the data set analyzed here. An alternative model is a power law plus a blackbody (Table A.4), where the thermal component could have a physical origin and be the hard tail of a Comptonized accretion disk. However, the values found in the present work are well above the value of 54^{+6}_{-4} eV found with *BeppoSAX*, but with a more complex model (Grandi & Palumbo 2004). On the other hand, 3C 273 appeared to be in a different state when observed with *BeppoSAX* and with *XMM-Newton* (see also Page et al. 2004).

3EG J1324-4314 (Cen A): Centaurus A is the nearest AGN in the sky ($d = 3.84$ Mpc) and has been observed twice by *XMM-Newton* with a delay of one year between the two observations. An analysis of these data has been published by Evans et al. (2004) and we refer the reader to that paper for more details, particularly for the extranuclear environment. But, since the purpose of the present work is to study the continuum, we performed the fit in the 4 – 10 keV energy band, to avoid the complex features in the low energy part of the spectrum. Moreover, to guarantee a good approximation of the continuum, we ignored the energy band 6 – 8 keV, which is affected by prominent emission lines. After having fixed the power law, the energy band of the iron complex is restored and one or two Gaussian emission lines are added to the model to complete the fit (Table A.6). Both observations require a Gaussian emission line from FeKα, but a wing toward the high energy is present. The addition of another large line with centroid at 6.8 keV determines an improvement in the fit of the ObsID 0093650201 (although the centroid is not well constrained), but not in the ObsID 0093650301 (it should be noted that this ObsID has less statistical power, because the MOS2 data are not useful). The iron complex found here is partially in agreement with the *BeppoSAX* results obtained by Grandi et al. (2003): the discrepancies refer to the FeKβ line at 7.1 keV, that is not required by the present data sets. The variability of the neutral iron line found by Grandi et al. (2003) is confirmed also by the present data: the line flux changed significantly between the two observations (spaced by 1 year), but increasing with the source flux increases, the opposite of what has been found in *BeppoSAX* data. However, two points temporally spaced by one year are not sufficient to claim different behaviour.

3EG J1339-1419 (PKS 1334-127): This flat-spectrum radio quasar has been poorly observed in hard X-rays: the only available observations are with *ROSAT* and *Einstein* (see, e.g., Maraschi et al. 1995a). The present analysis is also the first look at the hard X-ray emission ($E > 4$ keV) of this source. A simple power law model, with absorption in excess of the Galactic column, provides the best fit. The photon index is in the middle of the values from *Einstein* and *ROSAT* (Maraschi et al. 1995a), and consistent with both within the 90% confidence level.

3EG J1409-0745 (PKS 1406-076): This source was never studied in X-rays: *ROSAT* observation resulted only in an upper limit (2σ) with $F_{0.1-2.4\,\mathrm{keV}} < 2.35 \times 10^{-13}$ erg cm^{-2} s^{-1} (Siebert et al. 1998). *XMM-Newton* observed this blazar twice, with the second observation about one month after the first one, and the fluxes in the *ROSAT* energy band were 4.2 and 3.9×10^{-13} erg cm^{-2} s^{-1}, respectively. In both observations, the source was best fitted with a simple power law with $\Gamma \approx 1.6$ and no additional absorption.

3EG J1621+8203 (NGC 6251): This EGRET source has been associated by Mukherjee et al. (2002) with the nearby FRI radio galaxy NGC 6251 ($z = 0.02471$). Later studies supported this conclusion, e.g. Sowards-Emmerd et al. (2003), Chiaberge et al. (2003), Guainazzi et al. (2003), Foschini et al.

(2005). There is one *XMM-Newton* pointing available which lasted 50 ks, but heavy contamination with soft-proton flares strongly reduced the effective exposure on the three detectors (see Table A.1). The best fit model is an absorbed broken power law model. The addition of a thermal plasma to the single power law does not provide an improvement with respect to the broken power law model. This data set has been analyzed by Gliozzi et al. (2004) and Sambruna et al. (2004), but there are some discrepancies with the present analysis (mainly the presence of the FeKα emission line) likely to be attributed to a different cleaning of soft-proton flares. In the present analysis, the addition of a narrow (0.1 keV) or broad (0.5 keV) line at 6.4 keV, determines a worsening of the fit both with respect to the single and the broken power law model. On the other hand, the present results are consistent with *ASCA* and *BeppoSAX* observations analyzed by Chiaberge et al. (2003) and Guainazzi et al. (2003) that found no indication of any emission line of the iron complex. An improvement with respect to the single power law is obtained by adding the `mekal` model, but the fit remains always worse than the broken power law model. The parameters of the single power law plus thermal plasma model are: $N_{\rm H} = (1.16 \pm 0.08) \times 10^{21}$ cm^{-2}, $kT = 0.58^{+0.16}_{-0.13}$ keV, $\Gamma = 1.91 \pm 0.03$ for $\tilde{\chi}^2 = 1.02$ and 810 dof. The observed flux in the 0.4 – 10 keV energy band is 5.81×10^{-12} erg cm^{-2} s^{-1}.

*3EG J*1830 − 2110 *(PKS* 1830 − 211*):* This is the highest redshift blazar in the present sample ($z = 2.507$) and is gravitationally lensed by an intervening galaxy at $z = 0.886$ (Wiklind & Combes 1996, Lidman et al. 1999, Courbin et al. 2002). It was observed in the past in X-ray by *ROSAT* (Mathur & Nair 1997), *ASCA* (Oshima et al. 2001) and *Chandra* (De Rosa et al. 2005). The present data set has not yet been published and two observations of the three available are affected by high background.

3EG J2158-3023 (PKS 2155-304): This BL Lac object is the third calibration source in the present sample and, for this reason, it has been observed several times. Most of the present data set have been already published (Edelson et al. 2001, Maraschi et al. 2002, Cagnoni et al., 2004, Zhang et al. 2005), where it is possible to find more detailed analyses, particularly with reference to timing properties. This source, being one of the brightest in the X-ray sky, is also used in the search for the warm-hot intergalactic medium (WHIM) and a local absorber has been detected at 21.59 Å (≈ 0.57 keV) with the Reflection Grating Spectrometers (RGS) on board *XMM-Newton* (Cagnoni et al. 2004). However, since the study of this type of feature is outside the purpose of the present work, the spectrum of PKS 2155 – 304 has been fitted in the 0.6 – 10 keV energy range and then the flux has been extrapolated to 0.4 keV.

Table A.6. (*left*) Additional fit results for Cen A (3EG J1324 − 4314) with the model composed of an absorbed power law, plus one or two gaussian emission lines. Fit performed in the 4 – 10 keV energy band and then extrapolated to 0.4 – 10 keV. The two columns refer to the two observations. The rows list the following parameters: (1) Absorbing column density [10^{20} cm^{-2}]; (2) Photon index of the power law model; (3) Normalization of the power law model [10^{-2} ph cm^{-2} s^{-1} keV^{-1} at 1 keV]; (4) Energy of the emission line 1 [keV]; (5) Line width σ 1 [keV]; (6) Flux of the emission line 1 [10^{-4} ph cm^{-2} s^{-1}]; (7) Equivalent width of the emission line 1 [eV]; (8) Energy of the emission line 2 [keV]; (9) Line width σ 2 [keV]; (10) Flux of the emission line 2 [10^{-4} ph cm^{-2} s^{-1}]; (11) Equivalent width of the emission line 2 [eV]; (12) Reduced χ^2 and degrees of freedom; (13) observed flux in the 0.4 – 10 keV energy band [10^{-11} erg cm^{-2} s^{-1}]; (14) intrinsic luminosity in the 0.4 – 10 keV energy band rest frame [10^{45} erg s^{-1}]. The uncertainties in the parameter estimates are at the 90% confidence limit for one parameter of interest. For $N_{\rm H}$ = Gal, it means that the absorption column has been fixed to the Galactic value. The luminosities were calculated using d = 3.84 Mpc. (*right*) EPIC spectrum in the 4 – 10 keV energy band.

	0093650201	0093650301
$N_{\rm H}$	1420^{+40}_{-90}	1800 ± 200
Γ	$2.24^{+0.07}_{-0.04}$	2.3 ± 0.2
$A_{\rm pl}$	$22.1^{+0.3}_{-1.2}$	32^{+13}_{-10}
E_1	6.41 ± 0.02	6.44 ± 0.02
σ_1	< 0.074	< 0.065
$A_{\rm L1}$	$2.6^{+0.8}_{-0.6}$	$4.6^{+1.1}_{-1.0}$
EqW$_1$	70^{+22}_{-16}	107^{+26}_{-23}
E_2	$6.8^{+0.3}_{-0.4}$	-
σ_2	$0.76^{+0.39}_{-0.25}$	-
$A_{\rm L2}$	$4.3^{+4.4}_{-2.3}$	-
EqW$_2$	133^{+135}_{-71}	-
$\tilde{\chi}^2$/dof	0.99/984	0.96/498
F	17.4	18.5
L	3.1×10^{-4}	3.3×10^{-4}

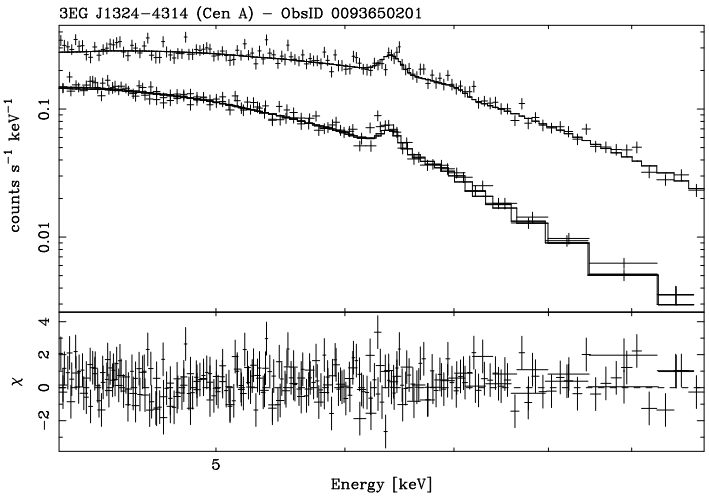

Table A.7. Optical properties of the AGN of the present catalog (from the Optical Monitor data). The data refers to the magnitude averaged over the whole observation. Columns: (1) Source name; (2) V magnitude [543 nm]; (3) B magnitude [450 nm]; (4) U magnitude [344 nm]; (5) UVW1 magnitude [291 nm]; (6) UVM2 magnitude [231 nm]; (7) UVW2 magnitude [212 nm]; The uncertainties in the parameter estimates are at the 1σ level and also include systematics.

Name	V	B	U	UVW1	UVM2	UVW2
(1)	(2)	(3)	(4)	(5)	(6)	(7)
0219 + 428				15.1 ± 0.1		
AO 0235 + 164				17.0 ± 0.1		
PKS 0521 − 365						
S5 0716 + 714	13.4 ± 0.1		12.9 ± 0.1	12.8 ± 0.1	12.8 ± 0.1	
S5 0836 + 710	16.6 ± 0.1		15.9 ± 0.1	16.1 ± 0.1		16.5 ± 0.1
Mkn 421						
PKS 1127 − 145				15.7 ± 0.1	15.7 ± 0.1	15.9 ± 0.1
ON 231	14.6 ± 0.1	15.0 ± 0.1	14.2 ± 0.1			
3C 273	12.6 ± 0.1	12.9 ± 0.1	11.8 ± 0.1	11.5 ± 0.1	11.3 ± 0.1	11.3 ± 0.1
	12.7 ± 0.1	12.9 ± 0.1	11.7 ± 0.1			
				11.5 ± 0.1	11.3 ± 0.1	11.3 ± 0.1
	12.7 ± 0.1	12.9 ± 0.1	11.8 ± 0.1	11.5 ± 0.1	11.3 ± 0.1	11.3 ± 0.1
				11.3 ± 0.1	11.1 ± 0.1	11.1 ± 0.1
				11.4 ± 0.1	11.3 ± 0.1	
	12.7 ± 0.1	13.0 ± 0.1	11.8 ± 0.1	11.6 ± 0.1	11.5 ± 0.1	11.4 ± 0.1
Cen A*						
PKS 1334 − 127				16.3 ± 0.1	16.2 ± 0.1	
PKS 1406 − 076		19.5 ± 0.2		18.6 ± 0.1		19.7 ± 0.1
				19.4 ± 0.4		
NGC 6251		15.6 ± 0.1	16.4 ± 0.1	16.6 ± 0.1		
PKS 1830 − 211*						
PKS 2155 − 304						12.5 ± 0.1
						12.1 ± 0.1
						12.2 ± 0.1
	13.2 ± 0.1	13.4 ± 0.1	12.4 ± 0.1			
	13.9 ± 0.1	14.2 ± 0.1	13.2 ± 0.1			12.8 ± 0.1
	13.8 ± 0.1	14.2 ± 0.1		13.1 ± 0.1	12.9 ± 0.1	12.9 ± 0.1
			12.9 ± 0.1	12.7 ± 0.1	12.6 ± 0.1	
	13.5 ± 0.1		13.2 ± 0.1			
		14.3 ± 0.1		12.7 ± 0.1	12.6 ± 0.1	12.6 ± 0.1

* Source beyond the capabilities of OM: too faint or too bright.

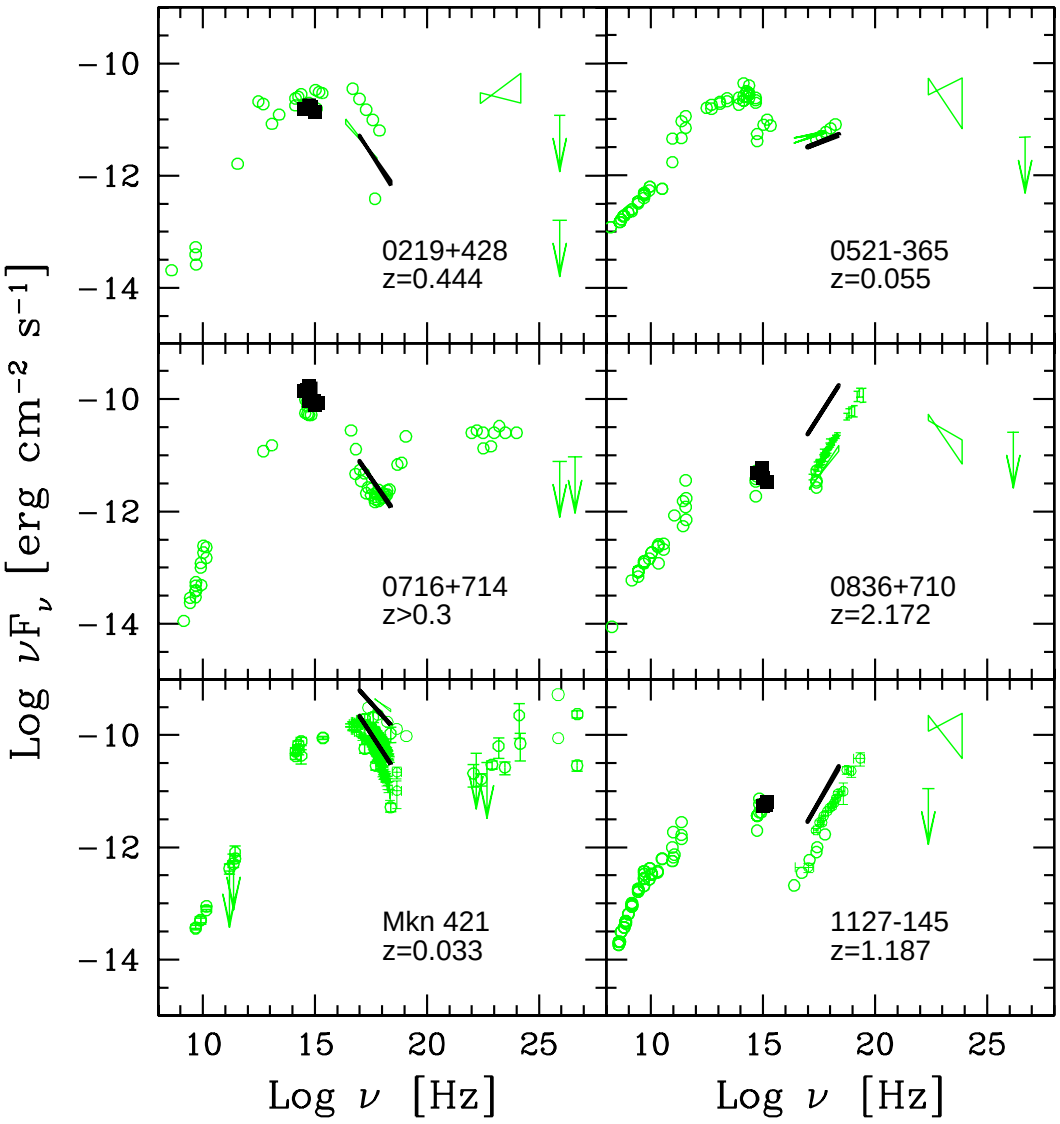

Fig. A.1. SED of the sources studied in this paper. We compare the *XMM-Newton* data (filled black symbols) to the available archival data in all bands.

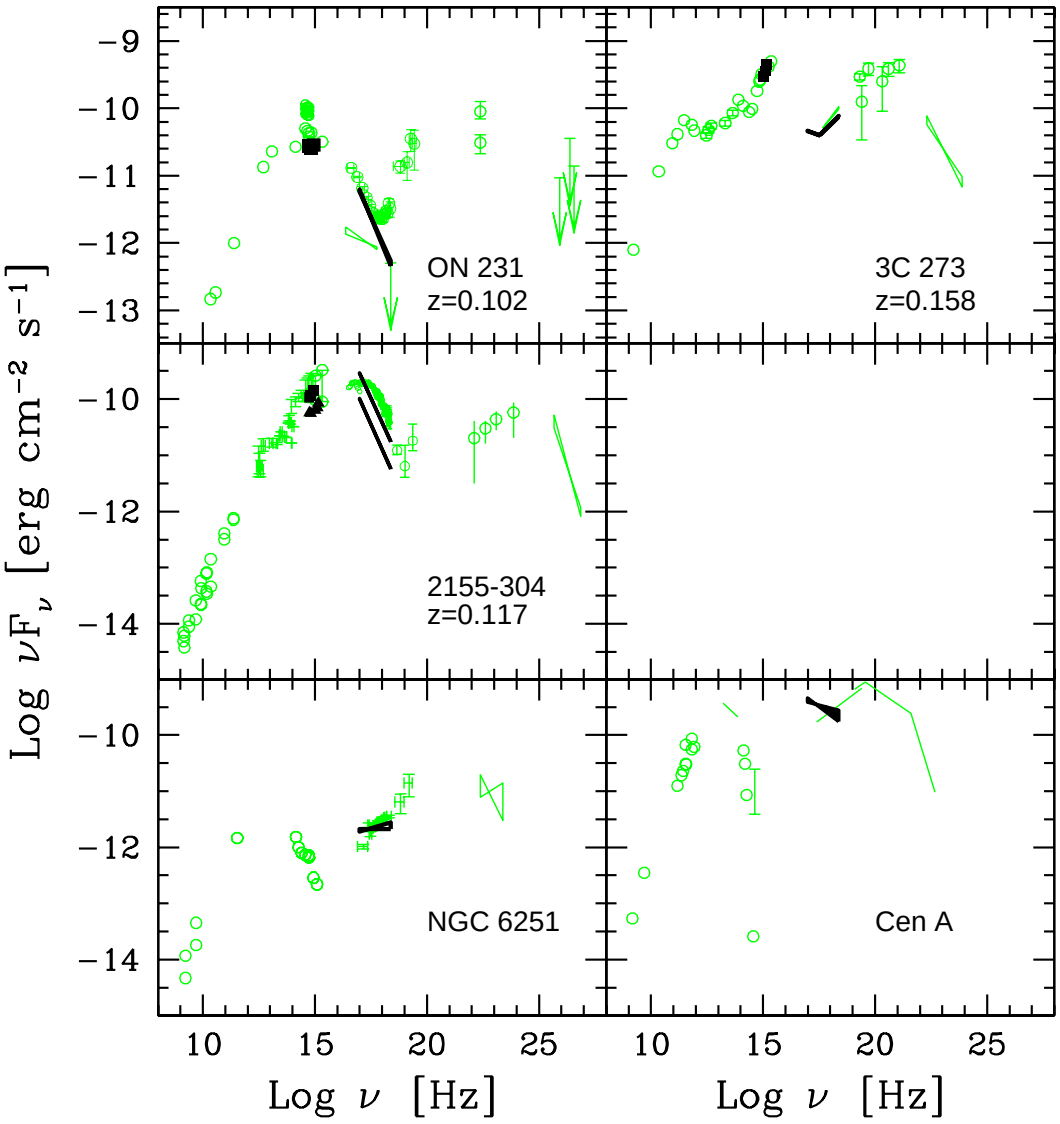

Fig. A.2. SED of the sources studied in this paper. We compare the *XMM-Newton* data (filled black symbols) to the available archival data in all bands.